8-2018

Feasibility Study of Thermal Treatment for Mercury Removal from Soils

Thomas Edward Spain
Clemson University, tspain@Clemson.edu

FEASIBILITY STUDY OF THERMAL TREATMENT FOR MERCURY REMOVAL FROM SOILS

A Thesis
Presented to
the Graduate School of
Clemson University

In Partial Fulfillment
of the Requirements for the Degree
Master of Science
Hydrogeology

---

by
Thomas Edward Spain
August 2018

Accepted by:
Dr. Ronald Falta, Committee Chair
Dr. Lawrence Murdoch
Dr. Stephen Moysey

ABSTRACT

Thermal remediation is an established method for the remediation of volatile organic compounds (VOCs). Thermal remediation for the remediation of elemental mercury was successfully applied by Kunkel et al., 2006 in the laboratory scale. Before the technology can be applied to the field scale, the thermal treatment for mercury needs to better understood using numerical simulation.

The Department of Energy's TOUGH2/TMVOC Code was developed at the Lawrence Berkeley National Laboratory and was used to evaluate the potential effectiveness of thermal treatment to remediate elemental mercury. TMVOC is a three phase non-isothermal numerical simulator for water, gas, and VOCs in porous media and was used to simulate the removal of elemental mercury due to its liquid state at 25°C and relatively high vapor pressure at elevated temperatures.

The overlying work was conducted as feasibility research for the maturation of thermal treatment for elemental mercury. Multiphase flow, contaminant phase change, and transport processes were investigated as mercury transfers from the liquid to gas phase and is then extracted from the system. Geometry, temperature, pressure and mass injection rates were evaluated to better understand the thermal treatment process for the treatment of mercury. The study consists of three key elements: 1) Numerical simulation of one dimensional thermal treatment experiments performed by Kunkel et al., 2006 for the treatment of elemental mercury 2) Simulation of ex-situ thermal treatment simulation under varying conditions for the removal of elemental mercury and 3) A feasibility

assessment of in-situ thermal treatment for the removal of elemental mercury in porous media.

ACKNOWLEDGMENTS

I would like to take the opportunity to acknowledge a few of the people who helped to make this work possible. First, I would like to thank Dennis G. Jackson at the Savannah River National Laboratory who funded the research presented in this work. Second, I would like to thank all the supervising committee members, Dr. Ronald Falta, Dr. Lawrence Murdoch, and Dr. Stephen Moysey for being present at my thesis defense.

Finally, I would like to thank my family, without their love and support the work presented here would not have been possible. Specifically, I want to thank my parents and sister who provided words of encouragement along the way.

TABLE OF CONTENTS

Page

Table of Contents (Continued) Page

LIST OF TABLES

LIST OF FIGURES

Figure Page

CHAPTER ONE

INTRODUCTION

1.1 Introduction

Mercury is one of the most toxic heavy metals and is used for its unique characteristics worldwide. Mercury is used in a wide variety of applications that range from dental fillings to barometers and engine manufacturing (Hutchison & Atwood, 2003). Elemental mercury is naturally occurring and has been listed as a priority hazardous substance for long atmospheric resonance, mobility and bioaccumulation (Alloway, 2012; Sierra et al., 2016) . Mercury cannot be degraded and therefore must either be removed or immobilized (Ochoa-Loza et al., 2001; Wang et al., 2012a).

Awareness of the negative effects mercury has on human health and environment has increased the need for regulation and remediation strategies (Xu et al., 2015). During the late 1980s the government began to recognize the need for regulation on mercury contamination and began to act accordingly. The United States Environmental Protection Agency (U.S. EPA) began to regulate the amount of mercury released into the air, water and wastes under the Clean Air Act, Clean Water Act, and the Resource Conservation and Recovery act (U.S. EPA, 2013).

The Oak Ridge Office of Environmental Management (OREM) has been addressing the mercury contamination at the Oak Ridge National Lab (ORNL) for decades. The Y-12 plant at the ORNL processed more than 11 million kg of elemental mercury during the 1950s-1960s to separate radioactive element isotopes (Peterson et al., 2015). Three percent of the 11 million kg of elemental mercury used at the Y-12 plant

was lost to the environment and presents a remediation challenge that is ongoing today (Brooks & Southworth, 2011). ORNL has developed and refined a conceptual site model for mercury (Brooks & Southworth, 2011; Looney et al., 2008); developed a strategic plan for mercury remediation (Wilkerson et al., 2013), and prepared a mercury technology development plan (Peterson et al., 2015). These documents discuss thermal technology for the treatment of both excavated and in-situ soils contaminated with mercury and the technology development plan (Wilkerson et al., 2013) elaborates on the need for further development of the thermal desorption technology. The term soil will be used to in this work to describe unconsolidated geologic material, made up of dirt, sand and rock and may contain water, gas and mercury.

1.2 Problem Objectives

The objectives of this research were three-fold. The first objective was to simulate the (Kunkel et al., 2006) experiments using TOUGH2/TMVOC (Pruess, 2008). The second and third objectives were to develop and explore ex-situ and in-situ models to simulate thermal remediation of elemental mercury under varying temperature, mass injection rates and to assess the feasibility of using thermal treatments under varying conditions.

The simulations in this research were conducted using the TOUGH2/TMVOC code integrated into the graphical user interface (GUI) PetraSim (Swenson & Hardeman, 2003). TMVOC is an extension of the TOUGH2 codes capable of calculating phase change and fluxes of air, water, and volatile organic compounds in in three dimensions.

TOUGH2/TMVOC model validation for mercury removal was conducted using Kunkel's (2006) in-situ thermal desorption (ISTD) experiments. The main goal of this part of the research was to validate the simulations of thermal treatment of elemental mercury and to understand the initial conditions, mercury equation of state, and the sources and sinks necessary to model thermal treatment for elemental mercury. Once working conditions were established for simulation the thermal treatment of mercury, ex-situ and in-situ models were simulated over a wide range of temperatures and mass injection rates. Varying remedial conditions provide necessary information for optimized mercury removal within a reasonable amount of time and under safe pressure conditions.

1.3 Problem Outline

Numerical simulation will be used to evaluate the potential of thermal treatment for the removal of mercury. The purpose of the study is to consider the viability of thermal treatment to remediate in-situ and ex-situ elemental mercury in soils such as those at ORNL.

The goal of this study is to design field scale application of thermal treatment for the remediation of elemental mercury and to deliver an evaluation of the parameters needs to simulate the removal in both the in-situ and ex-situ application of thermal treatment.

1.4 Thesis Structure

Chapter 2 will provide mercury background information and discuss the mercury contamination problem at the ORNL. Chapters 3 will describe the TOUGH2/TMVOC validation process and chapters 4 and 5 will outline the ex-situ and in-situ methods

developed for the remediation of mercury under conditions representative of the ORNL and discuss the numerical simulations for each process. Chapter 6 will discuss the feasibility of thermal treatment and provide suggestions for continued work with numerical simulation.

CHAPTER TWO

BACKGROUND

2.1 Introduction

This chapter provides background information on mercury, mercury fate and transport at the ORNL and introduces thermal remediation. The first two sections will focus on the general properties of mercury. The remaining sections will describe the history and severity of mercury contamination at the ORNL and introduce the modeling sensitivities for the thermal treatment of mercury under conditions representative of the ORNL.

2.2 Mercury Properties

Mercury is a naturally occurring element that can be found in the environment in various organic and inorganic species. Most species of mercury are toxic to humans and pollution is a global concern because of mercury's mobility in the atmosphere, and long residence time (Wang et al., 2012b; Xu et al., 2015). Over the past century, several thousand tons of mercury have been released into the environment from several different sources (Bizily et al., 1999). Both Natural and anthropogenic activities release mercury into the environment and contributed to global mercury pollution. Natural activities include the weathering of the mineral cinnabar, geothermal activity and volcanic eruptions (Xu et al., 2015). Anthropogenic sources of mercury resulting from the combustion of fossil fuels and increased atmospheric pollution ten times after the start of the industrial revolution (AMAP/UNEP, 2013).

2.2.1 Mercury Sources and Transport

Natural geologic processes release mercury into the environment and naturally occurring mercury can be found in soils worldwide. Once released from geologic material, mercury can reside in the atmosphere for four to six months before deposition (Wang et al., 2012b). Mercury emissions released to the atmosphere from natural sources is estimated to be 80-600 t/yr (Mason et al., 2012). After atmospheric transport, mercury is deposited in one of two ways. Wet deposition occurs when mercury returns to the earth's surface in rainfall and dry deposition occurs when mercury returns as a particle. The global average concentration of mercury in the soil is 0.58 -1.8 mg/kg with slightly higher concentrations in histosols and camisols (Kabata-Pendias, 2010). Industrial point sources and manufactured goods release approximately 1960 t of mercury on a yearly basis (AMAP/UNEP, 2013; Xu et al., 2015). According to the AMAP/UNEP global assessment of mercury (2013) the largest sectors in 2010 contributing to global mercury contamination were small scale artisanal gold mining (ASGM), combustion of fossil fuels, and the production of non-ferrous metals (Mason et al., 2012).

Figure 1 and Figure 2 show the locations with the highest mercury pollution and the industrial sectors that contribute to global pollution. Anthropogenic sources of mercury also include discarded thermometers, batteries, and fluorescent lamps which account for more than 40% of mercury emissions in North America (Xu et al., 2015).

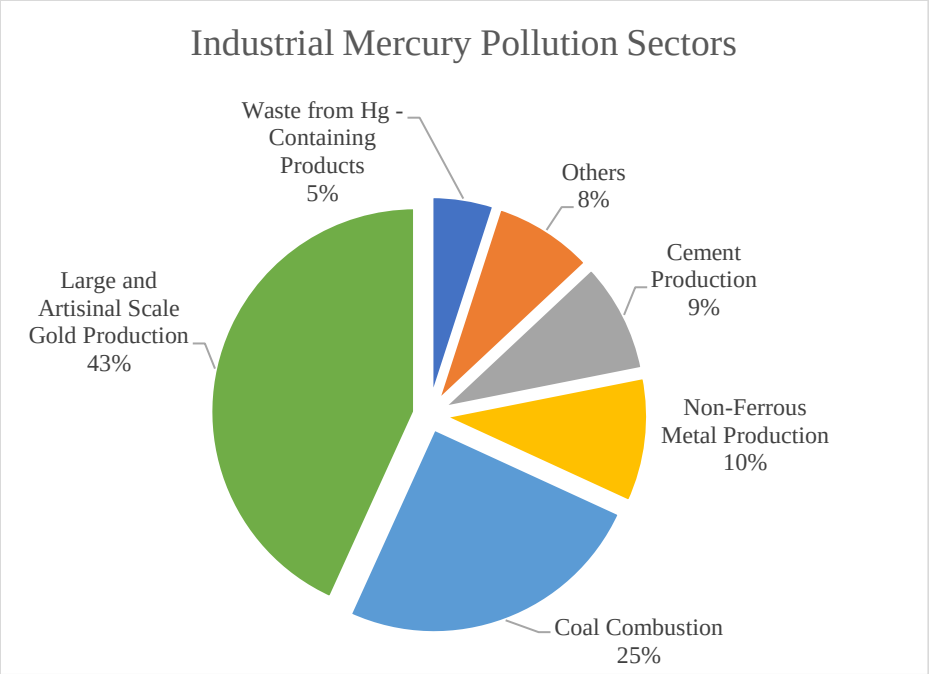

Figure 1: Global distribution of industrial pollution sectors for the year of 2010, modified from (AMAP/UNEP, 2013)

2.2.2 Mercury Toxicity and Health Effects

Most forms of mercury are toxic to humans and mercury is considered one of the most toxic global contaminants (Sierra et al., 2016; Xu et al., 2015). Humans exposure to mercury results from either ingestion or inhalation. When ingested, mercury affects the central nervous system and is most toxic to fetuses and children (Xu et al., 2015). Inhalation of mercury vapor can affect the circulatory system and cause tachycardia (Holmes et al., 2009). Mutter et al., (2004) reported that the elemental form of mercury has been linked to neurodegenerative disorders, such as Alzheimer's and Parkinson's disease. The inorganic forms of mercury have been documented to interfere with the immune system and kidneys (Holmes et al., 2009). The methylated form to mercury $[CH_3Hg]^+$ is considered to be the most toxic form of mercury to humans and has the ability to biomagnify in the food chain (Wang et al., 2012b). In aquatic environments,

methylmercury can accumulate in fish and then contaminate entire ecosystems. Species at higher tropic levels (humans) are then at greater risk of being exposed to mercury contamination.

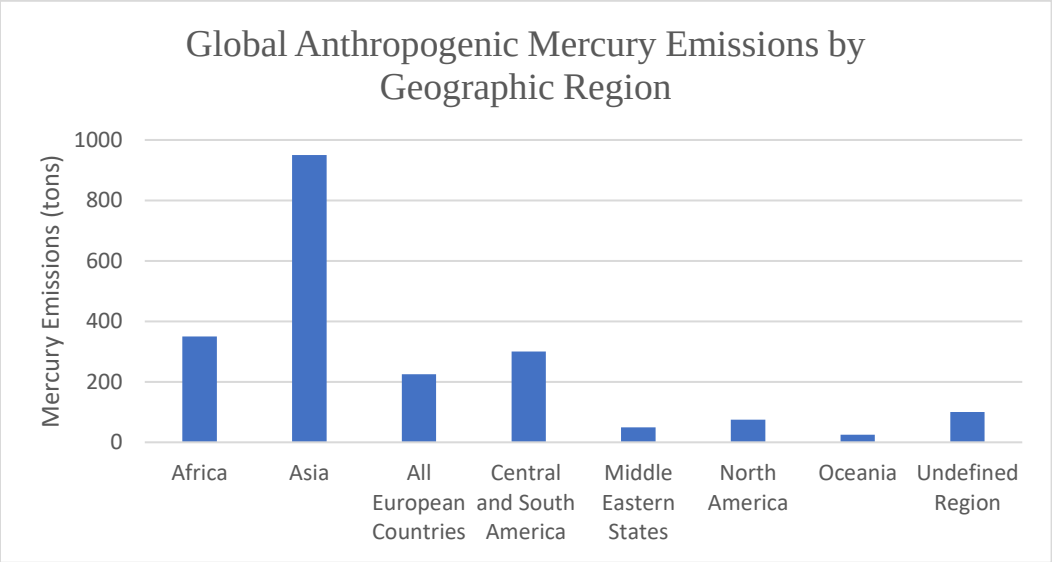

Figure 2: Global distribution of mercury pollution by geographic region for the year of 2010, modified from (AMAP/UNEP, 2013)

2.2.3 Vapor Pressure of Mercury

The vapor pressure of mercury has been documented as early as 1801 when the boiling point was first measured by Dalton (Dalton, 1802; Huber et al., 2006). Dalton recorded the boiling point of mercury to be 349°C and was reevaluated when Crichton (1803) recorded the normal boiling point to be above 346°C (Crichton, 1803; Huber et al., 2006). Over time the vapor pressure of mercury has been recorded with variable uncertainty due to temperature range of measurement, experimental method, and purity of mercury (Huber et al., 2006).

The Antoine equation may be used to model the vapor pressure of mercury (Equation 1) (Pruess & Battistelli, 2002):

$$\text{Ln } P_{vap} = A - \frac{B}{T + C}$$

Equation 1

is used. Where the constant values A, B, C, are empirical constants, and T is the temperature in Kelvin (Pruess & Battistelli, 2002; Reid, 1987). The coefficient values used in this study were obtained from the National Institute of Standards and Technology (NIST) and are recorded in Table 1 (Huber et al., 2006). The vapor pressure of mercury was calculated using Equation 1 and plotted in Figure 3. Vapor pressure curves indicate the temperature and pressure conditions in which liquid mercury evaporates into a gas. Points along the curve indicate the boiling point of mercury at a given temperature and pressure. Conditions above the curve indicate mercury in the liquid phase and conditions underneath represent mercury in the gas phase. Atmospheric pressure is represented in Figure 3 to indicate the normal boiling point of mercury. At one atmosphere of pressure, the normal boiling point of mercury is 356°C (629K). In presence of pressure greater than atmospheric the boiling point of a liquid is increased. This trend is represented by the upward positive trend in Figure 3. The reverse trend is also true. In the presence of a vacuum, or decreased pressure the boiling point of liquid can be decreased.

Vapor Pressure Empirical Constants		
Chemical Vapor Pressure Constant - VPB (Hicks, 1963)	11.1852	A
Chemical Vapor Pressure Constant - VPC (Hicks, 1963)	6924.17	B
Chemical Vapor Pressure Constant - VPD (Hicks, 1963)	-10.001	C

Table 1: Vapor pressure constants of mercury from Hicks, 1963 used to model mercury vapor pressure in the TMVOC numerical simulator.

The vapor concentration of mercury is calculated from temperature and pressure using the ideal gas law:

$$C_g = \frac{P_{vap} M_{wt}}{RT}$$

Equation 2

where C_g is the gas concentration, P_{vap} is the vapor pressure (Pa), M_{wt} is the molecular weight (g/mol), R is the ideal gas constant at standard temperature and pressure (R = 8314 cm^3Pa/mol*K). Sample calculations of mercury vapor concentration indicate that the concentration of mercury decreases with increasing temperature. At 100°C, 200°C, and 300°C the concentrations decrease from 6.53 kg/m^3 to 5.15 kg/m^3 and 4.25 kg/m^3. The volatility of mercury is the important thermophysical that allows it to be considered for thermal treatment. Mercury's high vapor pressure at high temperatures makes it an excellent compound to undergo thermally driven remediation techniques.

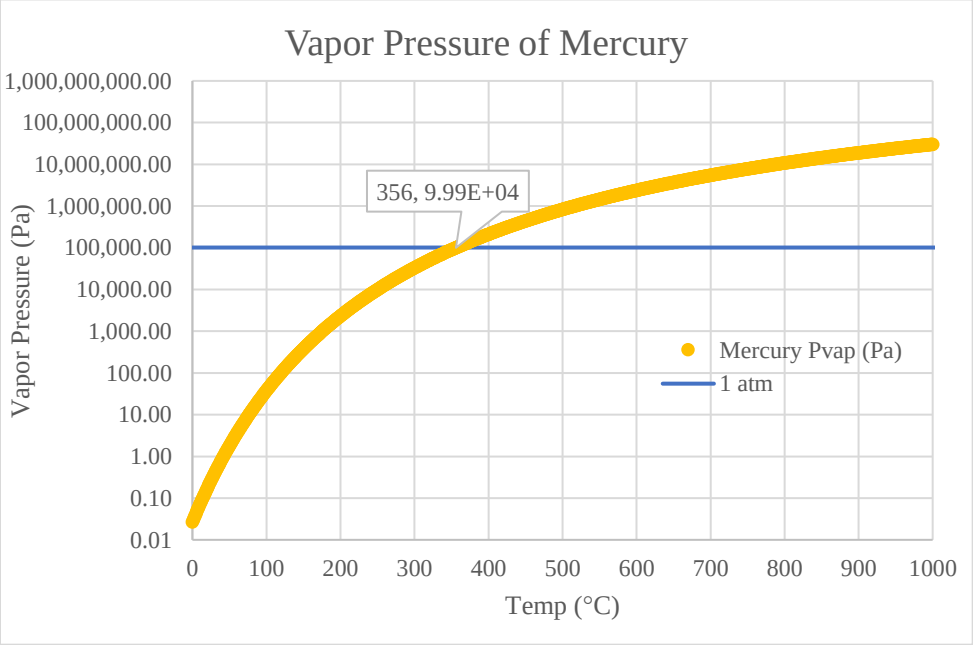

Figure 3: Vapor Pressure of Mercury calculated using Antoine's equation and vapor pressure coefficients from (Hicks, 1963)

2.3 Mercury at The Oak Ridge National Lab (ORNL)

The industrial complex located on the Oak Ridge Reservation (ORR) was originally built by the Clinton Engineering works in 1942. The complex of buildings was given the task to separate weapons grade uranium as part of the Manhattan project in 1940s and would later serve as the trial facility for plutonium separation in Handford, Washington (Brooks & Southworth, 2011). The X-10 plant at the ORNL was given the task of separating uranium-235 (235U) from 238U. After successfully separating uranium, an additional plant at the ORNL (Y-12) was given the task to separate lithium isotopes for the aircraft nuclear propulsion program (Brooks & Southworth, 2011).

The molten salt reactors required in the aircraft nuclear propulsion program required lithium-7 (7Li) because of its low neutron capture and its ability to impede the production of the salt reactor byproduct tritium (Brooks & Southworth, 2011). The naturally occurring lithium isotopes 6Li and 7Li can be separated using a mercury amalgam as described by Lewis and MacDonald in the 1930s (Brooks & Southworth, 2011; Lewis & Macdonald, 1936).

During the 1940s -1950s the demand for lithium isotopes increased drastically. The national Lab at Los Alamos began to request 6Li for weapons development (Brooks & Southworth, 2011). The United States then launched a high priority program to separate lithium at an industrial scale (Brooks & Southworth, 2011). Shortly after the Soviet detonation of a thermonuclear weapon in August 1953 the urgency for 6Li was at an all-time high. Several processes were designed to separate lithium, but all the processes required large amounts of mercury. During this time, mercury was a limited resource and research to find an alternative had begun. After no alternatives for mercury

were found, 6Li was separated using organic exchange (OREX), electrical exchange (ELEX) and column exchange (COLEX) processes (Brooks & Southworth, 2011). COLEX operations proved to be the most efficient at separating 6Li with the least amount of mercury and the Y-12 plant was converted from a uranium separation plant to a COLEX plant to produce 6Li at the industrial scale. The Y-12 plant would then use more than 11 million kg of elemental mercury during the 1950s-1960s (US-DOE 2014). Three percent of the 11 million kg of elemental mercury used at the Y-12 plant was lost to the environment and presents a remediation challenge that is ongoing today (Brooks & Southworth, 2011).

2.3.1 Mercury Releases at ORNL

The Li enrichment process at the ORNL was considered to be a National priority during the years 1955 to 1963 and much of the world's supply of mercury was being used at the Y-12 Plant (Brooks & Southworth, 2011; Smith, 2009). During these years, it is estimated that approximately 350,000 kg (~ 3% of 11 million) of mercury was lost to the local environment surrounding the Y-12 Plant (Brooks & Southworth, 2011). The total amount of mercury lost to the environment has some degree of uncertainty due to sampling and analytical methods changing over time as well as incomplete/missing records (Brooks & Southworth, 2011) (Table 2). Mercury inhalation was a known hazard at the Y-12 plant, and the workers participated in a screening program to monitor exposure. Workers wore air purifying respirators and several large building fans were installed in the Y-12 plant to reduce the exposure to the toxic mercury gas. Waste gasses from the COLEX process at the Y-12 Plant released approximately 37,000 kg into the air

(Brooks & Southworth, 2011). At the time, the COLEX exhaust stacks lacked the necessary scrubbers to limit the amount of mercury released into the atmosphere. Additional waste gases were released into the atmosphere from a mercury recover furnace. A Herreshoff-type recover furnace was installed at the Y-12 Plant to recover mercury from catchment basins and contaminated soils (Brooks & Southworth, 2011). The mercury recovery furnace physically separates mercury from solid material and roasts the remaining portion to vaporize the mercury and condenses the mercury off gas (Brooks & Southworth, 2011).

Historical Losses of Mercury at the Y-12 Complex		
Mercury Losses to:	Major Pathways	Mercury Lost (Kg)
Air	Ventilation Systems	23000
East Fork Poplar Creek	Effluent to stream	109000
Complex Foundation/Ground	Spills	195000
New Hope Pond	Building Drains	7000
Unknow Accounts	Unknown	587000
Estimated Total Lost		921000

Table 2 Historical mercury losses at the Y-12 Complex and the environmental exposure pathways modified from (Wilkerson et al., 2013).

Mercury entered the soils underneath and surrounding the Y-12 plant through spills, leaks, and equipment failures (Brooks & Southworth, 2011). Most of the mercury was recovered from small scale spills, but there are eight documented events where mercury spills were so large that soil had to be excavated and brought to the Herreshoff furnace for recovery (Brooks & Southworth, 2011). It is estimated that 193,000 kg of mercury was not recovered from the large spills and it is thought that less than two percent lost to the ground was recovered (Brooks & Southworth, 2011). It is believed that most of the mercury migrated through the karst network beneath the Y-12 Plant.

The Y-12 plant was built in the Bear Creek Valley near the headwaters of the East Fork of the Poplar Creek (EFPC) (Figure 4). The storm drain system at the Y-12 plant discharges into several small tributaries on the EFPC. Cooling water, building sumps, and cracked pipes at the Y-12 contribute to the industrial wastes and effluent reaching the EFPC and contaminating the surrounding area (Brooks & Southworth, 2011). The location where the Y-12 drainages enter the EFPC is called Outfall 200 (Brooks & Southworth, 2011). Outfall 200 is located upstream of Lake Reality, a small lined surface impoundment that replaced the New Hope Sedimentation Pond in 1988. Lake Reality was acting as a point source for mercury contamination in the EFPC until flows were diverted (Brooks & Southworth, 2011).

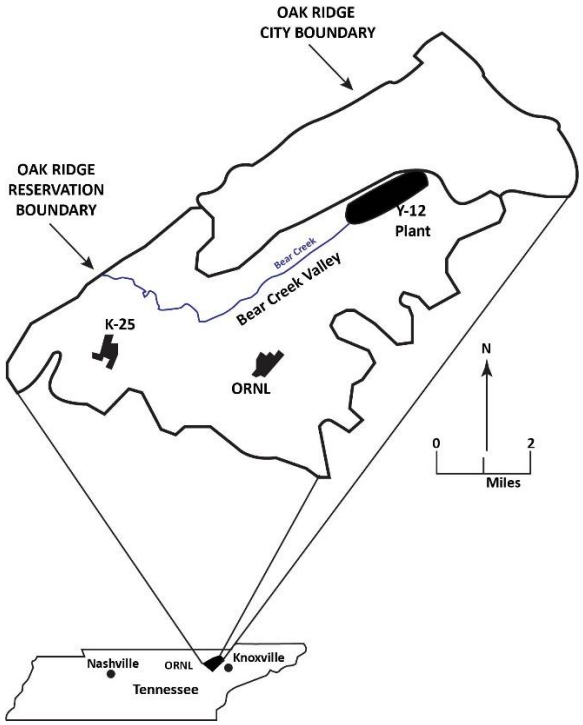

Figure 4: Geographic location of Bear Creek Valley, Tennessee modified from Sutton & Field, (1995).

During the COLEX processes at the Y-12 plant, mercury was placed in a nitric acid in preparation for lithium separation (Brooks & Southworth, 2011). The nitric acid dissolved small amounts of mercury and is believed to be the major source of contamination to the EFPC (Brooks & Southworth, 2011). Once the nitric acid rise was used for the preparation of mercury it was neutralized and discharged into Outfall 200 (Brooks & Southworth, 2011). Over time, a small amount of mercury dissolved in the acid accumulated in Outfall 200. In 1957, historical mercury concentrations estimate that mercury discharge in the EFPC peaked at 33,000 kg/yr (Brooks & Southworth, 2011).

2.3.2 Mercury Regulation

The ORR has a long history of mercury remediation in the soil, surface water, and shallow groundwater (Table 3). In 1989, the ORR was placed on the National Priorities list as a Superfund site under the Comprehensive Environmental Response, Compensation and Liability Act (CERCLA) (Brooks & Southworth, 2011). According to CERCLA, The Department of Energy (DOE), U.S. Environmental Protection Agency (U.S. EPA) and the State of Tennessee would act as governing bodies in the Federal Facility Agreement (FFA) at the ORR (Brooks & Southworth, 2011; Why, 2009). The FFA is required to develop and conduct the remediation activities at the ORR. The major role of the FFA is to make Record of Decisions (RODs) based on the Investigations under CERCLA. The RODs include: 1) a Phase 1 ROD for Interim source control of mercury in the Upper EFPC and; 2) a Phase II ROD for the Interim Remedial Actions for contaminated soils and scrapyards in the Upper EFPC (Brooks & Southworth, 2011; Why, 2009) The two key elements to the Phase I and Phase II RODs with respect to the

Integrated Facilities Disposition Project (IFDP) includes the remedial actions in the Upper East Fork of the Poplar Creek (UEFPC) and the deactivation and decommissioning of the Alpha and Beta buildings at the Y-12 Plant (Why, 2009).

Timeline of Mercury Clean Up Actions at the Y-12 Complex				
Years	Project	Significant Actions		
1985 - 1995	Building Remediation	Eliminate Mercury sources	Decontamination of Facilities	
1986 - 1987	Strom Drains	Storm Sewer Cleaning and Relining	Storm Sewer Relining	Drain Sediment Removal
1988 - 1989	New Hope Pond Closure	Unlined Settling Basin	Closed and Capped in 1989	
1988 - 1995	Pipe Replaced	610m of the North/South Pipe Replaced		
1992	Tank Remediation	13,610 kg of Mercury was removed form 3 settling tanks		
1994	Pant Effluent Hg Reduction	Storm Sewer Cleaning and Relining	Reroute Process Water	Water treatment at Outfall 51
1996 - present	Flow Augmentation	Flows altered to protect stream quality per 1995 NPDES Permit		
1996 - present	Central Mercury Treatment System	Mercury Treatment using Granular Activated Carbon (GAC)	Treats Contaminated Sump Water	
1996 - 1997	EFPC Floodplain Soil Removal	1995 Record of Decision	Public Input raised cleanup level	
1997	Basin Remediation	Mercury /PCB basin demolished and filled		
2001	Bank Stabilization	CERCLA Treatability Study	Stabilized Stream Bank	Reduced Mercury Releases
2005 - present	Big Spring Water Treatment System	Mercury Treatment System		
2009 - present	Ongoing Projects	Multiple Projects Under ARRA-Funding	Storm Sewer Cleanouts	Legacy material Removal

Table 3: Chronology for the mercury cleanup efforts at the Y-12 Complex from 1985 to present modified from (Wilkerson et al., 2013).

Performance standards outlined by the CERCLA RODs include a 0.2 µg/L standard of mercury discharged, as well as a fish tissue standard of 0.3 mg/kg (Why, 2009). According to The Tennessee Department of Environment and Conservation (TDEC), the Total Maximum Daily Load (TMDL) for mercury in the EFPC will be based on the fish tissue standard even though it is unclear how the fish tissue standard will be converted to a water quality standard (Why, 2009).

The long-term monitoring of mercury concentration is critical to understand mercury processes in the EFPC. Mercury concentrations in EFPC are monitored by B&W (BABCOCK & WILCOX) Y-12's Environmental Safety and Health Organization and Bechtel Jacobs Water Resources Restoration Program (BJC's WRRP) (Why, 2009).

B&W Y-12's routine monitoring is guided by the Tennessee Department of Environment and Conservation's Clean Water Act (CWA) National Pollutant Discharge Elimination System (NPDES) permit requirements, while BJC's requirements are dictated by CERCLA ROD - based performance measures (Why, 2009).

The first step in addressing the contamination at the Y-12 plant involved a Technical Readiness Assessment (TRA). TRAs are constructed to address commination, determine the development stage, and decide if remediation technology is developed enough for execution (US Department of Energy, 2009). The TRA was based on key assumptions as well as background and technical information (Looney et al., 2008). The stepwise technical assessment includes: (1) developing assumptions, (2) develop a site specific conceptual model and working hypothesis, (3) establishing science and technology targets, (4) delineating subdomains on specific conditions, uncertainties, and opportunities, (5) assessing scientific needs and environmental opportunities for each domain (Looney et al., 2008).

The TRA includes the Technology Maturation Plan (TMP). The US DOE and the National Aeronautics and Space Administration (NASA) have developed the nine-level maturity scale to determine the readiness of a remediation technology (US Department of Energy, 2009). The maturity scale is designed to lower risk of a remediation technology before full scale deployment. lower levels on the maturity scale have high risk, and higher numbers have low associated risk. The first two levels of the TMP scale include the conceptual model and the initial site characterization outlined in the TRA (US Department of Energy, 2009). Once a conceptual model has been created, potential

remediation efforts are evaluated. Feasibility research is the third step and includes the simulation work shown here for thermal remediation of mercury. The fourth through sixth levels include technology development at the meso scale and technology demonstration at the field scale. The seventh through ninth include engineered scale development and full-scale deployment (US Department of Energy, 2009).

2.3.3 Clean Up Efforts at ORNL

Past remediation efforts for the mercury problem at the Y-12 Plant include the Reduction of Mercury in Plant Effluents (RMPE) (Looney et al., 2008). Phase I ROD for the mercury source control included the multi-stage program designed to identify waterborne mercury sources in the EFPC and reduce the total daily mercury load to less than five gm/day (Brooks & Southworth, 2011; Looney et al., 2008).

The first step of the RMPE program included isolating and removing sources of waterborne mercury, and second treating mercury discharges (Looney et al., 2008). The sources of waterborne mercury were first prioritized by loading (g/day) and second by concentration (µg/L) with initial efforts focused on treatment of high loading and high concentration sources (Looney et al., 2008).

The RMPE program succeeded in reducing the mercury concentration in EFPC by more than 90% by the year 2000 (Brooks & Southworth, 2011). RMPE reduced the waterborne mercury by capping New Hope Pond, renovating storm drains, treating surface and sump water, and bank stabilization on the EFPC (Brooks & Southworth, 2011; Looney et al., 2008). In 2001, the RMPE program ended as waterborne mercury concentrations appeared to be stable in the EFPC (Brooks & Southworth, 2011). During

active years, total mercury concentrations in water in the uppermost reaches of this EFPC decreased from ≅ 1 ug/L to ≅ 0.5 ug/L and concentrations in the fish tissue decreased from ≅2 ug/g to ≅ 0.6 ug/g (Looney et al., 2008)

In addition to the implementation of RMPE and past technology initiatives at Y-12, continued source reduction and characterization activities are needed as part of the CERCLA baseline activities (BJC) (Why, 2009). Monitoring programs and research activities are essential for addressing mercury remediation and abatement in East Fork Poplar Creek (EFPC) and are needed to evaluate the success/failure of actions relative to CWA and TMDL requirements (Looney et al., 2008).

The Phase II ROD for the interim remedial actions for contaminated soils and scrapyards in the Upper-EFPC has been the recent focus of the FFA. IFDP remediation strategies for mercury contaminated soil and debris at Y-12 consider all of the harmful aspects of contaminated materials including, removing, handling, treating, and dispositioning contaminated material. The strategies also provide conceptual approaches to alternatives for D&D, remedial actions, and waste disposal (Why, 2009). Recent conceptual models discuss treatment of mercury contaminated soil and debris using low temperature thermal desorption (LTTD) (Peterson et al., 2015; Why, 2009). However, further research needs to be conducted to evaluate thermal desorption as a viable means of remediation for the contaminated soils and scrapyards in the UEFPC.

2.4 Mercury Remediation Practices

Comprehensive understandings of site geology, hydrogeology, hydrology, and physiochemical properties of contaminants are needed to assess the suitability of specific

remedial actions. The more that is understood about a site location the greater the ability to predict the mobility and distribution of a contaminant and develop a process for mitigation (Hinton & Veiga, 2001). After establishing an understanding of the contaminate and its surroundings, toxicity needs to be addressed so that the remedial measures do not cause further impact to ecological and human health.

In the past, mercury was disposed of in landfills. Recent knowledge of the hazards associated with mercury has developed more environmentally conscious methods for dealing with mercury contamination. Remediation actions can be divided into two categories based on the where the mercury is located when it is treated. Ex-situ remediation methods entail the excavation of contaminated material and above ground treatment, while in-situ remediation methods treat contamination in place.

Both ex-situ and in-situ remediation methods have their advantages and disadvantages. In-situ remediation techniques for elemental mercury have been less developed due to uncertainties in the subsurface and ex-situ methods disrupt contaminated areas. Further research is needed to constrain the remediation methods so that they may become more cost effective, have shorter durations and prevent more exposure to the environment.

There are two main methods used to remediate mercury contamination. The methods include immobilization, and separation. Each remediation method has processes that can be implemented either ex-situ or in-situ.

Immobilization remediation aims to transform mercury into a less toxic/stable species and to reduce species transportation (Conner, 1990). Immobilization consists of

stabilizing mercury species by using chemical immobilization and or physical barriers. Stabilization and solidification are both ex-situ forms of chemical immobilization where chemical additives are added to the soil to reduce the toxicity and mobility of a certain chemical species. One example of chemical immobilization is the injection of sulfur compounds to form mercury sulfide (HgS) (Hempel & Thoeming, 1999; Siebert, 2005).

Physical separation of contaminated sediments is an ex-situ remediation method driven by mercury's affinity for smaller particles (Hinton & Veiga, 2001). During physical separation, contaminated soil is removed and placed through a series of sieves. The smallest sediment particles are then rinsed of their mercury and the rinsate is retreated (Hinton & Veiga, 2001). Thermal treatment is type of separation that utilizes the thermophysical properties of volatile compounds to separate elemental mercury from mercury bound to solids. Chemical separation is an in-situ process where chemical leaching increases the solubility of certain compounds. Increasing the solubility of compounds promotes transportation within the subsurface and the mercury can be removed using pump and treat methods. Chemical separation has been most effective in areas where the ground water is contaminated with mercuric chloride ($HgCl_2$).

Thermal treatment of mercury utilizes heat to increase the vapor pressure and increase the volatility of mercury (Wang et al., 2012a). The small amount of waste volume associated with thermal treatments has been a driving factor in the increased popularity of thermal treatments. Once a contaminate has been volatilized and removed from a contaminated volume, the vapors need to be treated in an off-gas treatment system. All other contaminated material is left in place and after treatment is virtually

contaminate free. Thermal treatments have been successfully applied to organic contaminants and can be scaled for mercury recovery in soil. Mercury has been successfully treated using thermal methods within the temperature range of 127 – 700°C with greater efficiently at higher temperatures (Chang & Yen, 2006; Kunkel et al., 2006; Massacci et al., 2000).

Thermal remediation for mercury can be implemented in both ex-situ and in-situ applications. Ex-situ thermal treatment is the most common for mercury in the pilot and full scale (He et al., 2015). Drum and rotary kilns are heated to temperatures that exceed 500°C and contaminants are evaporated and recondensed outside of the previously contaminated volume. The off gas must then be treated. This approach can be quite costly due to excavation and transport, health and safety requirements. Metal repartitioning and altered physical properties of soil has presented problems with this current method. Running thermal treatments at longer times and at a reduced temperature has been one suggested method to combat the repartitioning of heavy metals and reduce the metals impact on environmental quality (Qu et al., 2004; Wang et al., 2012a). In-situ application of thermal treatment incorporates a heat source (hot air injection) alongside soil vapor extraction (SVE) wells to remove volatile contaminants from a control volume. This approach to thermal treatment for elemental mercury will be modeled in this research and applied to both ex-situ and in-situ applications.

2.5 In-situ and Ex-situ Thermal Treatments

2.5.1 Thermal Treatments

Thermal treatments are not a new technology when it comes to treating soils contaminated with organic compounds. Thermal treatments have been successfully used to remediate soil contaminated with volatile organic compounds, semi volatile compounds, polychlorinated biphenyls, and dioxins (de Percin, 1995). Commercial development of rotary kilns utilizing thermal treatment has been successful by numerous companies including: Econ Industries, SepraDyne-Raduce, PMET, Remedial Technology Group and X-Trax (Ebadian, 2001; Morris, 2002; Mulligan et al., 2001; Stepan et al., 1995). Problems associated with rotary kilns include contaminate redistribution during transportation and mercury condensate fouling rotary equipment (Ebadian, 2001; Stepan et al., 1995). These issues drive the effort for the development of ex-situ methods that are less complicated and less expensive.

Rotary kilns utilize heating temperatures of 1000°C and are often placed in areas where the temperature differences require special insulation, maintenance, and large operating costs (Hempel & Thoeming, 1999). The physical crushing of contaminated material required to use rotary kilns can also be costly when large volumes of building rubble needs treatment. The contamination of complex rotary kiln equipment also needs to be addressed for large scale remediation. These limitations in ex-situ thermal treatments have been the driving factor behind the feasibility research presented here.

In-situ vapor extraction methods also present a few scope and scale problems. ISTD units require the installation of heating wells surrounding an extraction well. These complex systems require costly drilling and large sections of insulative barriers to retain heat and prevent vapors from escaping the drawdown areas of the vacuum extraction

wells. Heat is applied to well casings and only the areas near the wells are heated conductively (Stegemeier & Vinegar, 2001). Injecting hot air convectively heats up the contaminated area and does not require porewater to transfer heat.

The University of Texas was donated the patents for in-situ thermal desorption (ISTD) technology in 2000. Since the donation, laboratory and modeling research has been conducted to test the thermal remediation technology for mercury. Early efforts by Lambert (2000) indicated 99.6% of mercury was recovered in contaminated column experiments (Siebert, 2005). More recent work by Kunkel et al., (2006) indicates greater than 99.8% mercury removal. The experiments performed by Kunkel et al., (2006) were used as a basis for a validation simulation conducted in this research.

2.5.2 In-situ Thermal Desorption (ISTD) and Soil Vapor Extraction (SVE)

Soil vapor extraction (SVE) is a process used to remove contaminants from subsurface soil using vacuum (Stegemeier et al., 2005). Soil heating vaporizes volatile compounds and the vacuum forces air through the unsaturated zone to recover water and contamination (Stegemeier et al., 2005). The Kunkel et, al. (2006) ISTD column experiments were based off ISTD processes with the addition of vacuum extraction.

A typical in-situ soil ISTD and SVE remediation system may include multiple heater wells, staggered in rows and columns or placed in geometric patterns, surrounding at least one vapor extraction well (Stegemeier et al., 2005). The distance between the wells depends on the well's radius of influence and the rate of injection and pressure applied at the vacuum. Vacuum wells are typically applied at a soil/air interface or placed within the soil to entrain air and volatilized contaminants (Stegemeier et al., 2005). The

off-gas captured from the vacuum extraction may then include contaminants which may need to be treated in an offsite treatment facility. Off gas mercury vapor is highly toxic needs to be captured in a safe manner before transport and treatment. Minimizing the escape of mercury vapor is of the utmost importance and needs to be considered when progressing the technology described in this work.

Convective heating is the primary means of heating the soil to the temperatures high enough to volatilize contaminants and does not rely on soil water to transfer heat. Several methods used to heat soil include electrical resistance heaters placed in wellbores, heat transfer fluid circulated through a wellbore, combustion within a wellbore, and the injection of hot air (Hinton & Veiga, 2001; Stegemeier et al., 2005). Alternatively, hot air will be used as the heat source in the models described in Chapters 4 and 5. Convective heating from injected air will heat up the simulated volume and vaporize mercury contamination.

In ISTD and SVE systems, a barrier may be included to define a treatment area and to prevent the escape of contaminate vapors (Hinton & Veiga, 2001). Barriers may be incorporated into the system to prevent fluid from migrating out of the treatment area and to inhibit water recharge. A common barrier used in ISTD systems are thermal blankets. Thermal blankets are constructed from a low permeability, insulative material used to prevent vapor from escaping the treatment area. Thermal blankets cover the treatment system and maximize the amount of contaminated airflow extracted to the surface by enhancing lateral airflow through a contamination zone. Vacuum ports in the thermal

blanket allow the contaminated air to flow out of the vacuum wells and prevent vapors from escaping through soil pathways at the surface (Hinton & Veiga, 2001).

The ISTD and SVE remediation systems outlined in this section as well as the Kunkel et al., (2006) column experiments will provide a base set of criteria to construct the thermal remediation models outlined in this work. Kunkel et al. (2006) utilize heaters to raise the temperature of the column and SVE to extract mercury off-gas. The major difference in the thermal treatment models outlined is the heat source. Hot air with an enthalpy defined at a specific temperature is used to heat of the contaminated volumes. Injected air and SVE wells will be applied to engineered systems outlined in Chapters 4 and 5 for both the ex-situ and in-situ systems.

2.6 Sensitivities for Thermal Treatment

Thermal treatments are affected by contaminant volatility and the amount of airflow pathways present in the soil. The amount of airflow channels within the soil is based on gas saturation and capillary pressure. In addition, soil temperature, treatment time, and heating rate are also important operating factors that influence the decontamination processes and will be the major parameters recorded to determine the feasibility of using thermal treatment for the remediation of mercury (Bucala et al., 1994; Lighty et al., 1988; Saito et al., 1998).

Water content and the permeability of the soil are two important factors that need to be considered when designing thermal treatment applications. Both the water content and the permeability may limit the effectiveness of ISTD and SVE. Water is present in soil and may occupy a fraction, or all of the porespace. In the vadose zone water occupies

a fraction of the pore space and shares the residual with gas and present contamination. The interface between the vadose zone and an aquifer is referred to as is the water table. Porewater impedes the movement of the other phases present due to relative permeability effects. Areas of low permeability that influence the horizontal and lateral flow of water through the vadose zone or an aquifer are called aquitards. The permeability of a soil may limit the effectiveness of SVE. SVE applies a vacuum to capture soil vapor so that it is extracted out of a particular area. Soil that contains high permeability regions has airflow that bypasses low permeability regions (Stegemeier et al., 2005). Low permeability regions reduce gas and fluid migration and can be defined as areas containing fine grain material. Low permeability regions are present in fractured and stratified geologic formations and can contain large amounts of contamination after air flows around these regions. Heat delivered by ISTD may vaporize the pore water within the vadose zone. The proximity to the water table needs to be considered as the influx of water due to capillary forces can hinder subsurface temperatures from exceeding the boiling point of water. Once the porewater has boiled, temperatures within the volume can increase to evaporate mercury. The absence of porewater increases permeability and additional pathways for airflow to evaporate mercury.

2.7 Summary and Goals of the Work

Thermal treatment technology has the potential to remediate both excavated soil and in-situ contaminated soils. Application of in-situ thermal desorption to remediate compounds (organic) is common but its application for mercury has only been tested as the laboratory scale (Kunkel et al. 2006), under ideal conditions. The purpose of the study

will be to consider the viability of thermal treatment to remediate in-situ and ex-situ elemental mercury. The research delivered in this study can be used to assess the potential to use thermal treatments for mercury at the field scale.

CHAPTER THREE

MODEL VALIDATION

3.1 Introduction

The goal of Kunkel et al., (2006) was to evaluate the feasibility of using thermal remediation to remove elemental mercury from soils. Laboratory experiments were developed to understand air flow and temperature behavior on sediment columns contaminated with mercury.

The column experiments were transitioned over to mercury as the contaminant effluent profiles can be scaled as a function of vapor pressure (Kunkel et al., 2006). The first objective of this study is to validate the TOUGH2/TMVOC numerical simulator to model Kunkel's (2006) thermal treatment of elemental mercury.

3.2 TOUGH2/TMVOC

TOUGH2, a general-purpose simulation program was developed by the Lawrence Berkeley National Laboratory (Pruess, 2008). The TMVOC numerical simulator calculates three phase multidimensional flow and models heat as well as contamination transport and behavior in unsaturated zones (Pruess & Battistelli, 2002). The TMVOC simulator mode was chosen to replicate the Kunkel experiments (2006) for its ability to track the mobility of contaminants through porous heterogeneous saturated and unsaturated media (Pruess & Battistelli, 2002). Phase concentrations are calculated directly from the integral form of basic conservation of mass equations.

The general governing integral equation is used for conservation of mass and energy equations:

$$\frac{d}{dt}\int_{V_n} M^i dV_n = \int_{\Gamma} \vec{F} \cdot \vec{n} d\Gamma + \int_{V_n} q dV_n$$

Equation 3

Equation 3 integrates the mass and energy over a volume (V_n) which is bounded to a closed surface (Γ). The mass accumulation term (M^i) is on the left side of the equation and is calculated for the component (i) (water, chemicals, non-condensable gases and heat energy). $\vec{F}$ is the mass flux and $\vec{n}$ is a normal vector pointing perpendicular to the surface Γ, and q are the sources and sinks.

The mass accumulation terms for water and gas:

$$M^i = \emptyset \sum_{\beta} S_\beta \rho_\beta X_\beta^i$$

Equation 4

is calculated from the summation of all of the fluids in the β phase (liquid, gas, NAPL). Where $\emptyset$ is the soil porosity, S_β is the soil saturation in the β phase. ρ_β is the density of phase β and X_β^i is the mass fraction of component i in phase. Most TOUGH codes use mass units for component i in β phase, but TMVOC uses molar units. Chemicals, such as VOCs may accumulate on solids through adsorption. Adsorption is accounted for using:

$$M^i = \emptyset \sum_{\beta} S_\beta \rho_\beta X_\beta^i + (1-\emptyset)\rho_R \rho_w X_w^i K_d$$

Equation 5

Where ρ_R is the density of the rock grains, ρ_w is the density of the aqueous phase and X_β^i is the mole fraction of the chemical component i in the β phase. The heat accumulation term:

$$M^i = \emptyset \sum_\beta S_\beta \rho_\beta \mu_\beta + (1 - \emptyset)\rho_R C_R T$$

Equation 6

where μ_β is the specific internal energy in phase β, C_R is the specific heat capacity of the rock, and T is temperature.

The flux terms on the right of Equation 4 include advective flux, diffusive flux and convective and conductive heat flux. The advective flux

$$\text{Advective } F_\beta^i = \sum_\beta X_\beta^i \rho_\beta V_\beta$$

Equation 7

equals the summation of the products of the mole fractions of component (i), the densities and Darcy velocity in the β phase. The Darcy velocity V_β in the β phase is

$$V_\beta = -k \frac{k_{r\beta}\rho_\beta}{\mu_\beta} (\nabla P_\beta - \rho_\beta g)$$

Equation 8

where k is the absolute permeability, $k_{r\beta}$ is relative permeability, μ_β is the viscosity and

$$P_\beta = P + P_{c\beta}$$

Equation 9

is the fluid pressure in the β phase, and equal to the sum of the reference pressure (usually in the gas phase) and the capillary pressure ($P_{c\beta}$). The heat flux includes conductive and convective components. The heat flux

$$\text{Advective } F^i = -K\nabla T + \sum_\beta h_\beta V_\beta$$

Equation 10

includes K which is the thermal conductivity. h_β is the specific enthalpy in the β phase.

Diffusive flux is added as a variation of Fick's law of diffusion:

$$\text{Diffusive } f_\beta^i = -\emptyset S_\beta \tau_\beta D_\beta^i \rho_\beta \nabla X_\beta^i$$

Equation 11

where $\tau_\beta$is the tortuosity and equals $\emptyset^{1/3}S_\beta{}^{10/3}$, and D_β^i is the molecular diffusivity of component (i) in phase β.

The integral finite difference method allows for the flexibility when establishing coordinate systems within TMVOC (Pruess & Battistelli, 2002). Time is calculated as a fully implicit first order backwards finite difference with upstream weighting of flux terms to prevent limitations in time steps (Pruess & Battistelli, 2002).

The TMVOC numerical simulator assumes three-phase local and thermal equilibrium based on several key assumptions. The multiphase system is assumed to contain water, a non-condensable gas (NCG) and water soluble volatile organic chemicals (VOCs) (Pruess & Battistelli, 2002). For the simulations modeled in this study, the NCG is assumed to be air. Any combination of the three phases may be present during the simulation.

The mechanisms that drive phase mass transfer within TMVOC are boiling and evaporation, dissolution of liquids in to the aqueous phase and the condensation of volatile chemicals from the gas phase into the non-aqueous liquid phase (NAPL). Liquid mercury within the volume starts to evaporate as injected air heats up the volume. Once mercury starts to evaporate, small zones of mercury vapor may condense on cool zones on the injection periphery. The contaminated area must experience enough hot air at high enough injection rates to overcome mercury condensation. Phase flow is calculated by a multiphase extension of Darcy's Law in response to gravity and pressure and includes the effects of relative permeability and capillary pressure between phases (Pruess & Battistelli, 2002). Heat is transferred during the simulation from conduction and multiphase convection.

3.2.1 Mercury in TOUGH

The VOC library in TMVOC does not include mercury. In order to simulate the thermal treatment of mercury, mercury needed to be created within the numerical simulator. The properties listed in Table 4 are used to establish mercury within TMVOC. The parameters are briefly discussed to better understand what needed to be defined in TOUGH2/TMVOC.

The molecular weight of mercury is 200 g/mol. The reference density, or specific gravity indicates the mass of mercury in 1 m^3. The normal boiling point of mercury is the temperature at which the vapor pressure is equal to atmospheric conditions. The critical temperature and critical pressure from mercury is recorded when the liquid and vapor phases have the same density (critical state). The temperature for gas diffusivity denotes

the temperature at which the molecular diffusivity for mercury is recorded. The reference temperature is the temperature where the density is measured. The reference binary diffusivity of mercury in air is proportionality factor in Fick's law of diffusion.

The critical volume is the amount of volume occupied by a unit mass of mercury vapor in its critical state. The critical compressibility is a factor that relates the real behavior of mercury to vapor to ideal mercury vapor. The Pitzer's Acentric factor is a measurement of the non-sphericity of mercury molecules, higher factors indicate higher boiling points. The chemical diffusivity exponent is used to calculate chemical diffusivity and the water solubility constant is solubility of mercury in water.

TOUGH2/TMVOC Mercury Parameters		
Thermophysical Parameter	Value	Units
Chemical Molecular Weight - AMO	200	g/mol
Chemical Ideal Gas Heat Capacity Constant - CPA:	20.8	g/mol
Reference Density for NAPL - RHOREF	1.31E+04	kg/m^3
Chemical Normal Boiling Point - TBOIL	630	K
Chemical Critical Temperature - TCRIT	1765	K
Reference Temperature for Gas Diffusivity - TDIDRF	293	K
Reference Temperature for NAPL - TDENRF	520	K
Reference Binary Diffusivity of VOC in Air - DIFV0	7.36E-06	m^2/s
Chemical Critical Pressure - PCRIT	1510	bar
Chemical Critical Volume - VOLCRT	42.70	cm^3/mol
Chemical Critical Compressibility - ZCRIT	0.439	
Pitzer's Acentric Factor - OMEGA	-0.167	
Chemcial Diffusivity Exponent	1.92	
H2O Chemical Solubility Constant - SOLA	1.60E-07	

Table 4: Thermophysical properties used to create mercury in TOUGH2/TMVOC

The dynamic viscosity was calculated for mercury as a function of temperature and derived from Yaw et al., (1976) using (Pruess & Battistelli, 2002):

$$\mathrm{Ln}\mu = A' + \frac{B'}{T} + C'T + D'T^2$$

Equation 12

where constants A', B', C' and D' are empirical constants calculated and recorded from Reid et al., (1987) and T is temperature in Kelvin (Table 5) (Pruess & Battistelli, 2002; Reid, 1987). When constants A' and B' are set to zero, the Van Velzen et al., (1972) equation (Pruess & Battistelli, 2002):

$$\mu = Ce^{D/T}$$

Equation 13

is used to calculate dynamic viscosity. Where C is assigned to a reference viscosity and D is a reference temperature.

Mercury Viscosity Empirical Constants		
Liquid NAPL Viscosity Constant - VLOA (Reid, 1987)	0.00	A
Liquid NAPL Viscosity Constant - VLOB (Reid, 1987)	0.00	B
Liquid NAPL Viscosity Constant - VLOC (Reid, 1987)	1.00	C
Liquid NAPL Viscosity Constant - VLOD (Reid, 1987)	518.00	D

Table 5: Mercury viscosity constants from Reid, 1987 used to calculate the viscosity as a function of temperature

The vapor pressure of mercury was estimated in each grid block in the TOUGH2/TMVOC simulation using Antoine's equation (Equation 1) (Pruess & Battistelli, 2002). Vapor pressure constants were obtained from the NIST database (Huber et al., 2006).

Capillary pressure and relative permeability are estimated using three phase methods modified from Parker (1987) and Stone (1970) (Pruess & Battistelli, 2002). Parker's three phase version of the Van Genuchten equation estimates capillary pressure using (Pruess & Battistelli, 2002):

$$P_{cgw} = -\left(\frac{\rho_w g}{\alpha_{gw}}\right)\left[(\overline{S_w})^{-\frac{1}{m}} - 1\right]^{\frac{1}{n}}$$

Equation 14

where P_{cgw} is the hydrostatic gas-water capillary pressure, ρ_w is the density of water, and g is the gravitational acceleration. Equation 14 assumes that there is no NAPL present; m = 1 - $\frac{1}{n}$; $\overline{S_w} = (S_w - S_m) / (1-S_m)$; and $\left(\frac{1}{\alpha_{gw}}\right) = \left(\frac{1}{\alpha_{nw}} + \frac{1}{\alpha_{gn}}\right)$.

The relative permeability values were determined using the modified version of Stone's three phase method (Pruess & Battistelli, 2002) (Equation 15, 16, 17).

$$k_{rg} = \left[\frac{S_g - S_{gr}}{1 - S_{wr}}\right]^n$$

Equation 15

$$k_{rw} = \left[\frac{S_w - S_{wr}}{1 - S_{wr}}\right]^n$$

Equation 16

$$k_{rn} = \left[\frac{1 - S_g - S_w - S_{nr}}{1 - S_g - S_{wr} - S_{nr}}\right]\left[\frac{1 - S_{wr} - S_{nr}}{1 - S_w - S_{nr}}\right]\left[\frac{(1 - S_g - S_{wr} - S_{nr})(1 - S_w)}{(1 - S_{wr})}\right]^n$$

Equation 17

Where k_{rg} is the relative gas permeability; k_{rw} is the relative water permeability S_g is the gas saturation; S_{gr} is the residual gas saturation; S_{wr} is the residual water saturation, and n is the relative permeability model fitting exponent.

3.3 Thermal Treatment Laboratory Experiments

The mercury experiments conducted by Kunkel in 2006 were performed in columns packed with silica sand. The columns were heated to temperatures between 243

and 259°C and mercury was injected into the middle of the column at a rate of 15 ml over 5 seconds (Kunkel et al., 2006). The mercury was injected through a sideward facing syringe aperture to promote outward migration of the mercury during injection. The pressure in the column was held close to atmospheric and vapor extraction was conducted at the top of the column.

3.4 TOUGH2/TMVOC Model

3.4.1 Solution Mesh

The first part of the simulation was to create a mesh and establish the initial conditions within the TOUGH2/TMVOC model. The TOUGH2/TMVOC models were setup to allow air to be injected at the bottom of the column and collected from the top using a one-dimensional grid (Figure 5). The 0.048m x 0.048m x 0.176m grid contains the same dimensions as the columns used by Kunkel et al., (2006) in the Hg3 mercury column experiments.

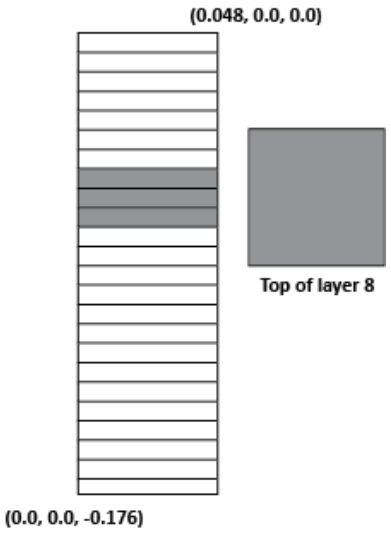

Figure 5: Mercury distribution in the TOUGH2/TMVOC simulation used to validate the thermal treatment of mercury from Kunkel et al., (2006) Hg3 simulation.

3.4.2 Layer Materials

The models described in this work contain porous media that was constructed to represent well sorted, rounded silica sand. The homogeneous porous fill material has a bulk density of 2600 kg/m^3 and a porosity equal to 0.31.

3.4.3 Initial Conditions

The initial temperature and pressure conditions within the column were 244°C and 101325 Pa (1atm). Kunkel et al., (2006) conducted the mercury Hg3 experiments at 244°C under standard pressure. At this temperature, the mercury vapor pressure is 0.084 atm. Before injection, air is the only initial phase within the column. The mole fraction of air in the column is 0.99 with the remaining 0.01 as water vapor.

3.4.4 Source and Sinks and Boundary Conditions

The second part of the simulation involves injecting the mercury into the column. Liquid mercury (1.1mL) was injected across the three contaminated grid blocks at rate of 1.00×10^{-4} kg/s for 50 s with an enthalpy of 3.415×10^4 J/kg.

The third part of the simulation is the post injection redistribution of mercury. Most the model gridblocks are located on the top of the contaminated zone and allow for the upward movement of the mercury as air is injected into the column. The grid blocks beneath the contaminated zone can show the initial downward liquid mercury migration post injection. However, the initial mercury saturation is below the residual saturation to prevent the mercury from migrating downward. The length and placement of the uncontaminated zone within the column does not impact the remediation time for the mercury (Kunkel et al., 2006).

The fourth and final part of the simulation was the injection of air into the column. In the TOUGH2/TMVOC simulation, air was injected after the mercury at a rate of 7.29 x 10^{-7} kg/s or 64 mL/min with an enthalpy of 2.45 x 10^{5} J/kg corresponding to 244°C. Water was also injected into the bottom layer of model to represent less than 1% humidity in the injected air. Water was injected as vapor at a rate of 1 x 10^{-9} kg/s with an enthalpy of 2.5 x 10^{6} J/kg. The top grid block in the TOUGH2/TMVOC simulation is held at constant temperature and pressure so air injected in to the bottom of the column can be produced from the top. Production wells can simulate the same results if the pressure gradient is not too large. Production wells were added to the ex-situ simulations to simulate the capturing of the off gas associated with a vapor extraction remediation system.

3.5 Simulation Results

The Kunkel et al., (2006) Hg3 experiment and the TOUGH2/TMVOC mercury extractions are illustrated in Figure 6.

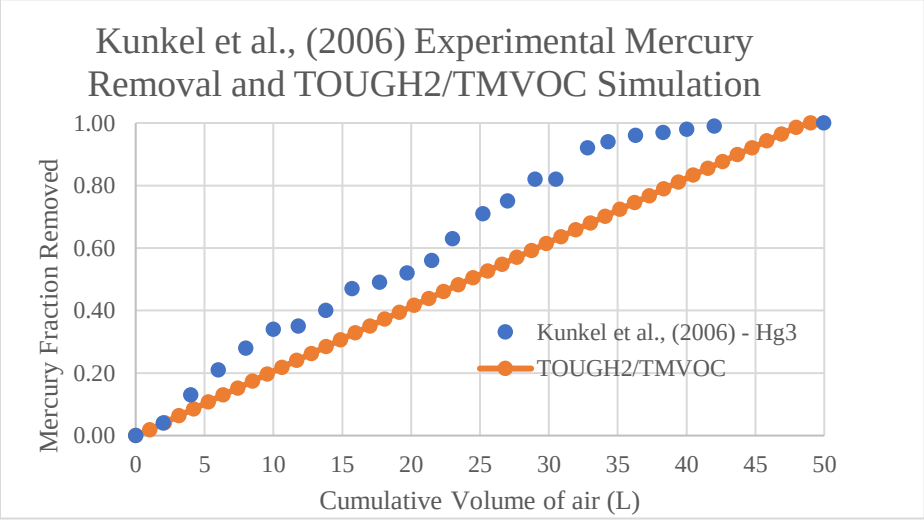

Figure 6: Kunkel et al., (2006) Hg3 experiment and TOUGH2/TMVOC mercury mass extraction.

The same air injection rate was used to validate the TOUGH2/TMVOC simulation assuming that all of the injected air is used to remove the mercury. However, the Hg3 simulation showed that 22% of the airflow bypassed the contamination zone through part of the column (Kunkel et al., 2006). The cumulative flushing volume and the air injection rate in the TOUGH2/TMOVC simulation were then reduced by 78% (Figure 7) to account for the flow bypassing the contamination zone in the Hg3 experiment.

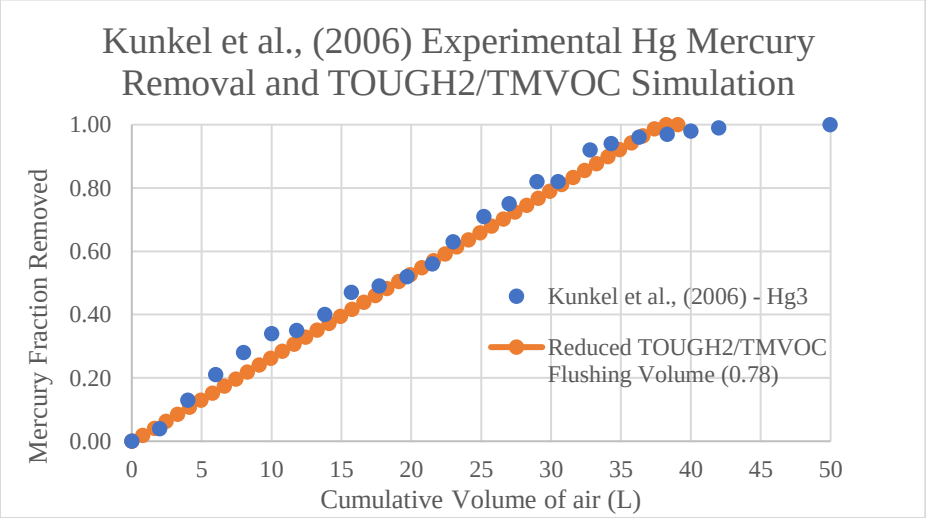

Figure 7: Kunkel et al., (2006) Hg3 experiment and TOUGH2/TMVOC mercury mass extraction with 78% air injection.

3.6 Conclusions

The TOUGH2/TMOVC numerical simulator can accurately model the thermal treatment of mercury using the injection of hot air. The model validation shown in Figure 7 indicates that the mercury extraction depends on the rate of injected air. Now that the TOUGH2/TMVOC numerical simulator has shown thermal treatment of mercury it will be used to construct ex-situ thermal treatment for elemental mercury.

CHAPTER FOUR

EX-SITU MODEL DESIGNS

4.1 Ex-situ Thermal Treatment

Ex-situ remediation methods treat contamination material that has been excavated from the source zone. One application of ex-situ treatment includes treating contaminated construction rubble and soil before transporting the debris to landfill. Although ex-situ treatment has a high risk for redistribution and exposure, the driving force is to treat disturbed soil.

Several proprietary methods remove mercury from construction fill using ex-situ thermal treatment (Mulligan et al., 2001). Mercury Recovery Services (MRS) and Chemical Waste Management Inc, are just two examples of companies use ex-situ thermal treatment for mercury (Mulligan et al., 2001; PMET, 2006). These current treatments options for elemental mercury have proven effective, however, they do have their disadvantages. Floess et al., (2011), describes ex-situ thermal desorption technologies used to treat soils contaminated with volatile organic compounds (VOCs), polychlorinated biphenyls (PCBs) and metals in rotary kilns (Floess et al., 2011). The main issue with rotary kilns is chemical condensate that forms in the off-gas system when organic chemicals in asphalt and roofing materials volatilize (Floess et al., 2011). Once a rotary kiln is fouled, cleaning the apparatus can be a timely process and potentially expose humans and redistribute contamination. The use of rotary kilns for treatment applications where contaminated sediments are mixed with building rubble may not be very cost effective (Floess et al., 2011; Mulligan et al., 2001). The disadvantages

associated with the rotary kiln ex-situ treatment options drives the need for the development of new ex-situ methods for the treatment of mercury.

Since the feasibility of thermal treatment will be assessed for the conditions representative of the ORNL, an alternative approach will be developed to clean up excavated contaminated materials such as the Y-12 plant demolition material. An idealized model was created in TOUGH2/TMVOC to simulate the removal of mercury from excavated sediments. A base case model was established and run under simplified geologic parameters at lower temperatures without using a rotating kiln.

The research goals addressed in this chapter concern the feasibility of thermal treatment for elemental mercury under varying temperature and air injection rates. The end assessment will discuss the conditions where mercury can be removed from ex-situ sediments under realistic conditions. The goal is to remove mercury from a variety of soils with different permeabilities. The ex-situ model was developed in the following steps: (1) model design (2) establishing the initial conditions within the volume, (3) heat and air flooding for the mercury removal, with vacuum production for the removal of mercury vapor.

The design of the model was derived from an outdoor oven and the flow conditions within the model were adapted from the model comparison preformed in Chapter 3. The air mass injection rate as well as the vacuum extraction rates were varied in order to extract mercury vapor in an effective manner and reduce pressure buildup within the system.

4.2 Ex-situ Simulations

4.2.1 Design

The ex-situ volume contains 50 m^3 of soil in a 5m x 5m x 2m rectangular basin (Figure 8). The soil represents excavated material that has been placed inside a container. The modeled system lacks an initial water saturation zone and a water table.

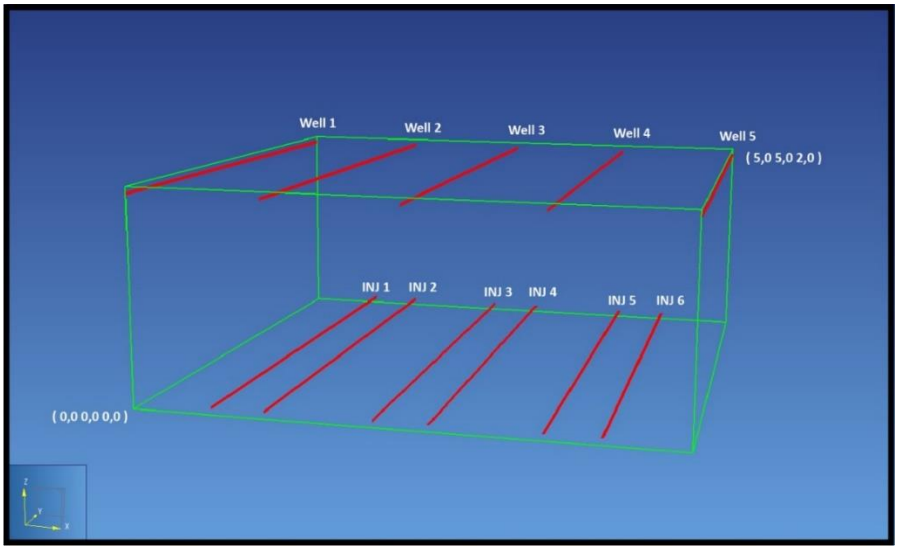

Figure 8: Ex-situ model (5m x 5m x 2m) represents a control volume of 50 m^3. Production wells (WELL) are located at the top of the model and Injection wells (INJ) are located at the bottom.

The cartesian grid contains gridblocks with a volume of 0.0625 m^3. The model contains 100 gridblocks in 8 vertical layers for a total of 800 gridblocks. The top and bottom of the model and the outer boundaries represent a sealed insulated material used to prevent heat and gases from escaping the system. Pressure buildup within the model was an important concern, as escaped mercury vapors present a large health hazard for workers in ex-situ thermal treatment. The only way for fluids to escape the model is through the production wells at the top of the model. Table 6 lists the simulation parameters and soil properties used to create the ex-situ model. The initial water saturation is 0.31 and the mercury saturation is 4.94×10^{-4} or 1157.51 mg/kg. The water

saturation remains close to residual (0.30), but mercury is immobile as the saturation is much lower than the 0.15 residual (Table 7). Maintaining initial water and mercury saturations close to the residual saturations reduces the mobility of the phases in the gravitational equilibrium models. The small residual gas saturation (0.01) ensures that the gas phase is the most mobile in the system. The material within the model was simulated to be unconsolidated homogeneous silica sand with a density of 2600 kg/m³ and a porosity of 0.31. The permeability is homogeneous through the system and is typical of coarse sand (1×10^{-11} m^2). The wet thermal conductivity of the soil is three times larger than the dry thermal conductivity. Since water is a better conductor than air the wet thermal conductivity of the soil is larger. Table 8 lists the parameters used to calculate the capillary pressure in Equation 14.

Ex-situ Base Case Simulation and Soil Properties		
Parameter	Value	Units
Initial Temperature	25	°C
Initial Pressure	1.01E+05	Pa
Porosity	0.31	
Soil Density	2.60E+03	kg/m^3
Wet Heat Conductivity	3.00E+00	W/(m·K)
Dry Heat Conductivity	1.00E+00	W/(m·K)
Specific Heat	1000	J/(kg·K)
Soil Permeability	1.00E-11 to 1.00E-13	m^2
Global Water Saturation	0.31	S_w
Global Gas Saturation	0.69	S_g
Global NAPL Saturation	4.94E-04	S_n

Table 6: Ex-situ base case simulation parameters and soil properties.

Soils of varying permeability were simulated to record the pressure build up in different types of porous material as a result of thermal treatment. The adsorption of

dissolved mercury to solids was neglected because of the mass is minor compared to the liquid elemental mercury. The horizontal wells within the model are defined in two separate categories. Production and injection wells were both incorporated into the model and allow for air to be injected into the model, and mercury vapors to be extracted from the top (Figure 8). The pressure within each vacuum well was held constant at a pressure less than one atmosphere. The constant well bore pressure within the extraction wells is used to remove vapors from the system. The injection wells inject air with an enthalpy adjusted for temperature desired to heat the volume. The air injected into the system was humid and water was injected at a rate proportionate to that of humid air.

Ex-situ Base Case Relative Permeability Parameters		
Relative Permeability Water Saturation Residual	0.3	S_{wr}
Relative Permeability Gas Saturation Residual	0.01	S_{gr}
Relative Permeability NAPL Saturation Residual	0.15	S_{nr}
Relative Permeability Model Exponent	3	n

Table 7: Ex-situ base case relative permeability parameters.

The well patterns illustrated in Figure 8 were established to provide ample hot air to the system and provide the extraction paths necessary to prevent accumulation of condensed mercury vapors in the corners of the contaminated volume. Constant rate heaters were added to the system in the base layer in some simulations to determine if the additional heat would improve mercury removal A base case model will be discussed in detail and then high, medium and low permeability cases are assessed. The base case model will use to evaluate and normalize the simulations so that the results can be compared to a standard.

Ex-situ Base Case Capillary Pressure Parameters		
Wetting Fluid Satuation Minimum	0.3	S_m
Capillary Pressure Model Exponent	1.5	n
Capillary Fringe NAPL and Gas	10	α_{ng} (m)
Capillary Fringe NAPL and Water	10	α_{nw} (m)

Table 8: Ex-situ base case capillary pressure parameters used in Equation 14.

The constant rate heaters delivered 20 J/s for a total of 1000 Watts in the base layer of the model. The heaters are included within the model as a source/sink and defined within the base layer gridblocks.

4.2.3 Wells

The parameters used to create the wells in the ex-situ models are listed in Table 9. The base case reference simulation injection rates are used to describe the following model. Air was injected into the model at a rate of 2.5×10^{-3} kg/s (219 L/min) over six wells with an enthalpy of 3.01×10^{5} J/kg corresponding to 300°C. The temperatures within TOUGH2/TMVOC are limited to the critical temperature of water (367°C) and the temperature of 300°C was chosen for injection.

Water is injected in the same 6 wells at a rate of 1/50th of the air injection rate to account for the air humidity. The 1/50th relationship is maintained for all of the mass injection rates used to simulate the thermal treatment of mercury. The horizontal injection wells were evenly spaced along the bottom of the control volume and screened to their entirety.

Ex-situ Model Well Parameters		
Parameter	Value	Unit
Injecition temperature	300	℃
Well radius (r_w)	0.0254	m
Effictive radius (r_e)	0.19947114	m
SVE Wellbore Pressure (P_{wb})	9.00E+04	Pa
Heaters	20	W

Table 9: Ex-situ base case well parameters.

Vacuum extraction wells were placed at the top of the volume. The vacuum wells were defined according to well deliverability and the pressure used to define a vacuum (Coats, 1977; Pruess & Battistelli, 2002; Thomas, 1982). The productivity index of a well is a parameter that relates the well production rate within a gridblock to the phase pressure when it is greater than the pressure within the wellbore (Coats, 1977). For radial flow within the gridblocks, the productivity index is calculated using (Coats, 1977; Thomas, 1982):

$$PI = \frac{2\pi(k\,\Delta z_l)}{\ln\left(\frac{r_e}{r_w}\right)}$$

Equation 18

where k is the permeability; Δz_l is the gridblock length perpendicular to the well; r_e is the effective well radius to the vertical gridblock area ($\sqrt{\left(\frac{(\Delta z \Delta x)}{\pi}\right)}$); and r_w is the well radius.

The pressure within the wells is held constant at 90,000 Pa. The vacuum wells were screened horizontally across the base layer and have a productivity index calculated using a two inch well, 0.5 m x 0.5 m x 0.25 m gridblock dimensions and a soil permeability of 1 x 10^{-12} m^2.

4.3 Base Case Ex-situ Simulation

The criteria used to determine the base case ex-situ model parameters were remediation time and pressure. The time necessary to remove mercury from the volume needs to be reasonable. The base case was chosen based on air injection rates that remove mercury in approximately two months with a maximum total pressure of one and a half atmospheres. The base case ex-situ model contains material with a moderate permeability of 1×10^{-12} m^2 and resembles a fine sand. The base case model and injection rate will be used to compare models with material permeabilities ranging in higher and lower orders of magnitude. Higher permeabilities are expected to require less time to remove the mercury and lower permeabilities are expected to take longer.

4.4 Ex-situ Base Case Results Simulation Results

The mass recovery was graphed for the base case simulation (Figure 9). The total mass of mercury (105 kg) and the total mass of water (4792 kg) within the volume was shown as air injection heats up the volume and water and mercury are vaporized (Figure 9). Once the mass of water has been removed from the volume the mass of mercury begins to drop.

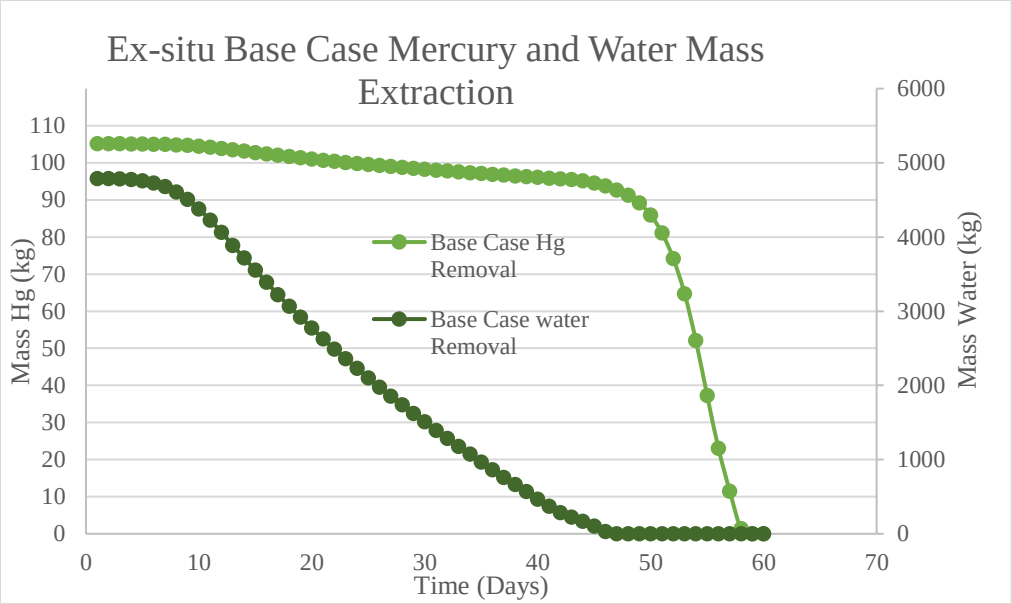

Figure 9: Mass extraction for ex-situ base case model. The mercury mass extraction is plotted on the left vertical axis and the water mass extraction on the right.

Temperature, pressure and various saturations values are several of the results that will be presented for the base case ex-situ simulation. The temperature within the volume is controlled by the enthalpy of injected air and the heaters in the base layer. The distribution of heat throughout the volume depends on the rate of mass injection as well as the wet and dry thermal conductivity of the porous fill material.

The temperature in the base case simulation varies over the course of the simulation time. The initial temperature within the system is 25 degrees and it heats up after 58 days of mass injection and constant rate heating. Figure 10 indicates the amount of heat that propagates through the volume at 13 days. The temperature increases in the areas where the hot air is being injected. The temperature scale in Figure 10 indicates the maximum temperature within the system does not exceed the temperature of the injected air. Once the air is injected, the energy is transferred to soil and the phases present. The

energy transfer within the system prevents the volume from reaching the same temperature of the injected air under the specified simulation time. Temperature within the volume increases until water begins to evaporate at 100°C. Once the water has evaporated, temperatures begin to rise about 100°C. The time necessary for the removal of mercury from the volume is 58 days under the described injection rates.

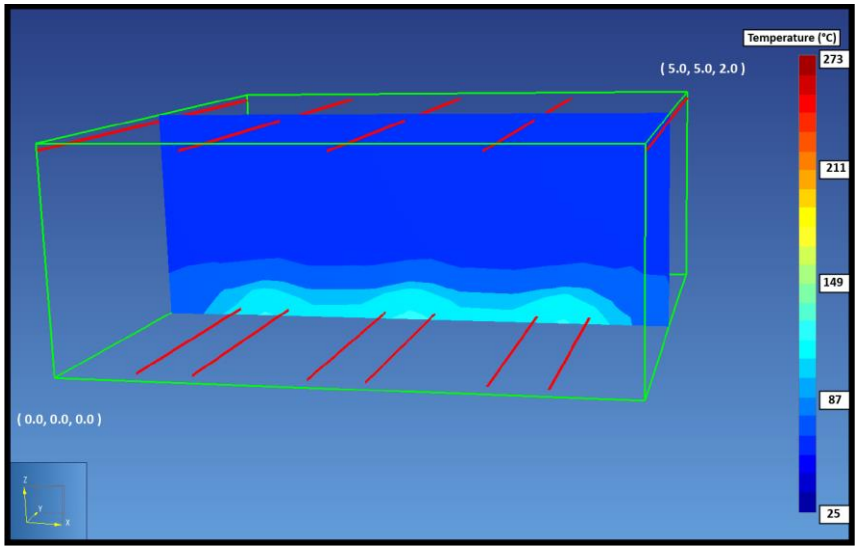

Figure 10: Ex-situ base case model temperature profile after 13 days of injecting hot air at a rate of 2.50 x 10^{-3} kg/s (243 L/min).

The amount of mass injection and the injection duration determines the maximum temperature within the volume and determines the rate of mercury removal within the system. Figure 11 illustrates the temperature within the system at 27 days. At this time the temperature gradient within the system starts to be altered by the SVE wells placed in the corners of the system. At the end of the Base Case simulation, the temperatures reached a maximum 268°C (Figure 12). The temperature recorded at 58 days represents the maximum temperature when mercury saturation in the volume is less than 1 x 10^{-5} everywhere. When mercury saturation falls below 1 x 10^{-5} everywhere only a residual

amount of mercury remains in the volume (0.04 kg/m^3). At this point, 98% of the mercury has been removed from the volume. The 3D temperature results of the base case simulation run without heaters indicate that the temperatures within the system are significantly lower when the base heaters are omitted from the system.

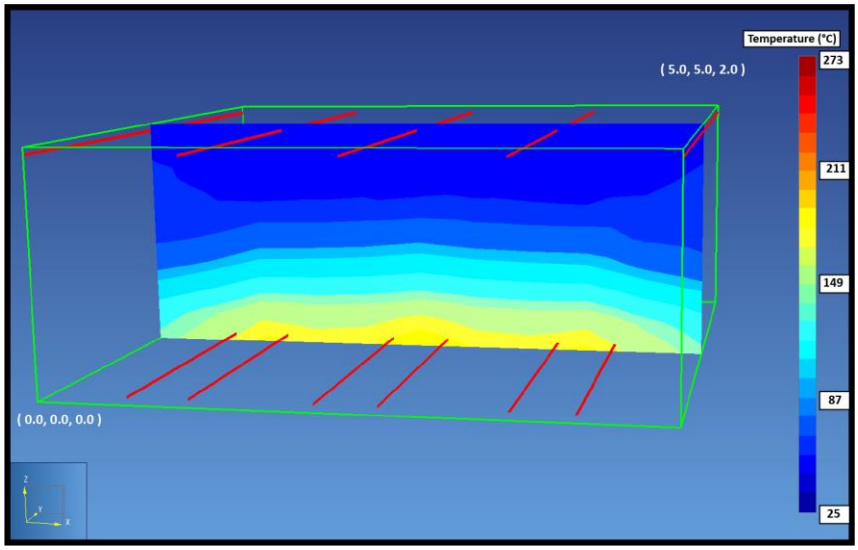

Figure 11: Ex-situ base case model temperature profile after 27 days of injecting hot air at a rate of 2.50 x 10^{-3} kg/s (219 mL/min). The base layer heaters are starting the influence the overall temperature of the control volume.

Figure 13 shows the total pressures in the base case simulation at 58 days. After 58 days the maximum total pressure within the gridblocks was 1.5 atm. A total pressure below 2 atms is reasonable to prevent mercury vapor escaping the system. The exact pressure criteria can be altered based on the container design.

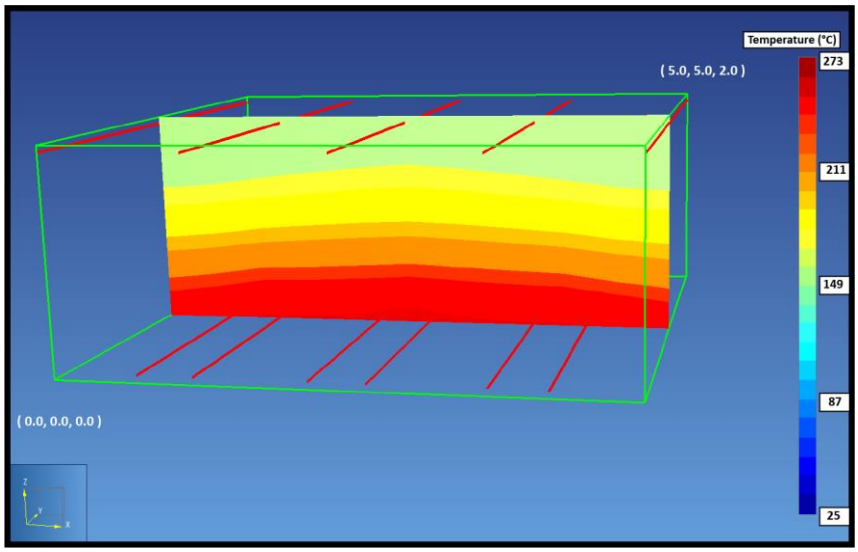

Figure 12: Ex-situ base case model temperature profile after 58 days of injecting hot air at a rate of 2.5 0 x 10^{-3} kg/s (219 mL/min).

The water and mercury saturation distributions are similar in-situ and ex-situ simulations. The injection of hot air drives evaporation through the volume that acts as the driving force for removing mercury from the system. As water evaporates within the volume, a small amount of mercury evaporates and condenses along the periphery of the water condensation front. Since water boils at temperatures much lower than boiling point of mercury the water needs to be completely removed from the volume before the majority of the mercury can be removed from the system.

The initial water saturation within the volume is 0.31 (Figure 14). The injection of hot air heats up the control volume and starts evaporating the pore water. Once pore water starts to evaporate, water saturation values in some parts of the volume exceed the initial saturation due to condensation in cooler regions. Figure 15 indicates water saturation of 0.31 above the heaters. The isosurface in Figure 15 indicates the water

saturation 0.31, saturations above the isosurface are greater than 0.31 and representative of water condensation.

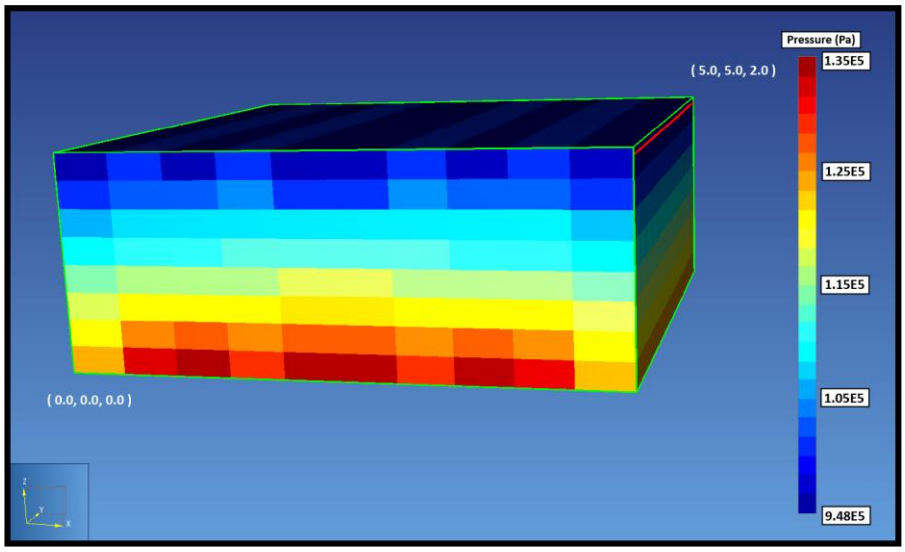

Figure 13: Gridblock total pressure values in ex-situ base case model after 58 days of injection.

After 18 days, the water condensation front within the volume starts to be altered by the SVE wells (Figure 16) The SVE wells #1 and #5 were placed adjacent to the no flow boundaries to prevent the accumulation of condensed vapor within the volume. At 26 days the simulation begins to show condensation between the wells. Apart from the continual condensation at the corners of the control volume, the water vapor is being produced from the SVE wells. After 47 days, the remaining liquid water has been removed from the volume (Figure 17)

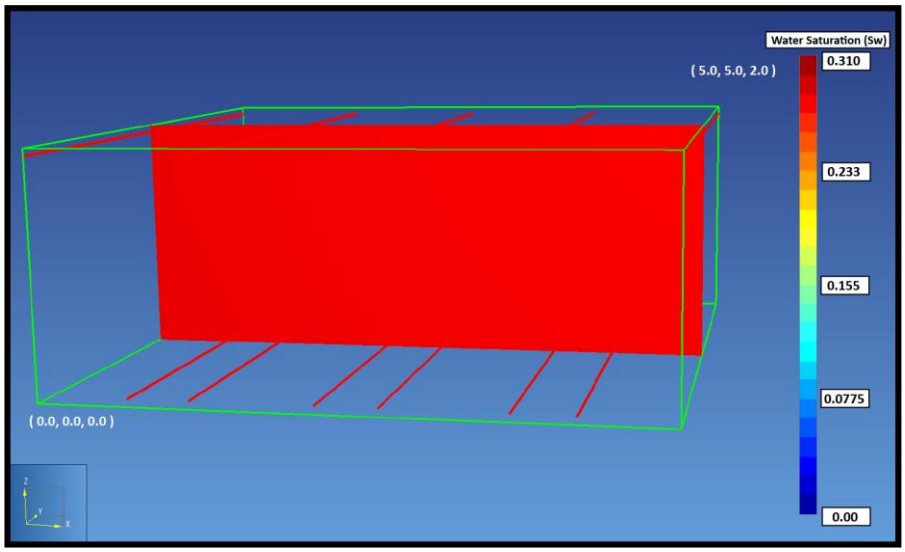

Figure 14: Initial water saturation (S_w) for the ex-situ base case model at time = 0 days. The S_w scale maximum is 0.31 and the three-dimensional results indicate the S_w= 0.31 is uniform before air is injection into the volume.

The liquid mercury saturation within the control volume is controlled by the evaporation front of the porewater. The water within the system must first evaporate before the local temperature can exceed 100°C. The initial saturation of mercury is 4.94 x 10^{-4} and equates to approximately 2 kg/m^3. The mercury undergoes a similar trend to the water saturation within the volume. Due to the condensation fronts the mercury saturation scale extends to a value larger than the initial saturation. After 8 days the mercury within the system begins to condense in some locations (Figure 18).

The mercury condensation front at 37 days is located under the SVE wells (Figure 19). Mercury also began to accumulate along the corners of the no flow boundaries parallel to the heaters and continued to follow this trend until all the mercury has been removed from the system. Figure 20 presents the accumulation of mercury in the same orientation of the heaters. After 55 days of injection the majority of the mercury is

removed but small amounts continue to condense in the cooler regions. After 58 days the volume is almost completely clean

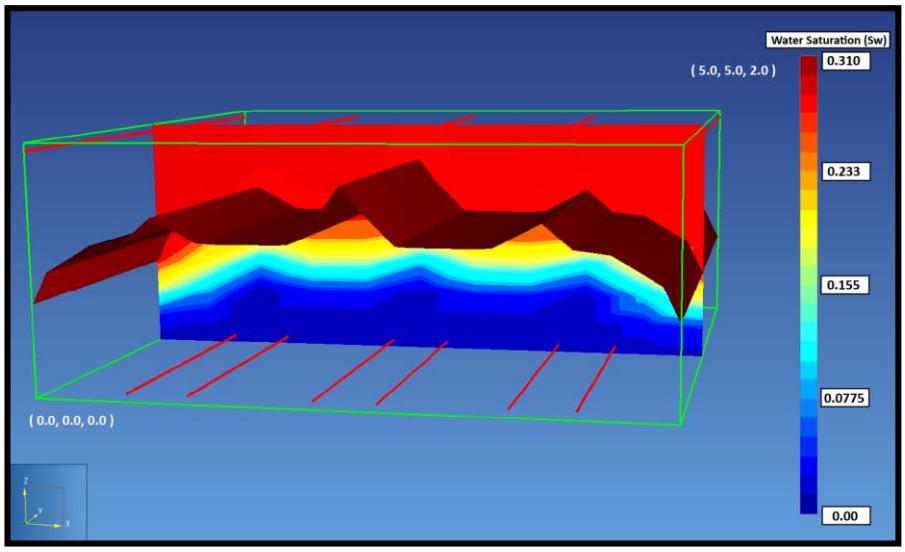

Figure 15: Water saturation (S_w) for the ex-situ base case model at time = 18 days. After 18 days, the condensation front within the control volume starts to be altered by the SVE wells. The isosurfaces indicates $S_w = 0.31$, the saturations above this surface are greater than 0.31 and representative of water condensation.

4.5 Ex-situ Discussion

The following simulation comparisons will be between the simulations that contain the same mass injection rates as the base case simulation. The altered variable compared between the following simulations will be presence of heaters and the permeability of the fill material. The effects of heat and the permeability of the fill material has effects on the temperature and pressure within the system and will therefore alter the amount of injection time necessary for the removal of mercury.

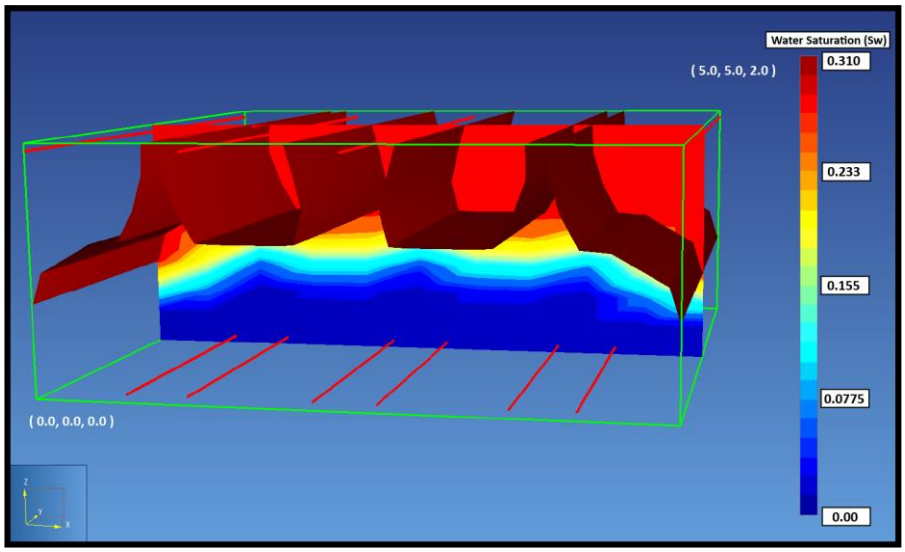

Figure 16: Water saturation (S_w) for the ex-situ base case model at time = 19 days.

4.5.1 Pressure

All of the ex-situ simulations were run with and without heaters. The pressure graph (Figure 21), list the simulations that contain the same air injection rate of the base case but contain varying permeability. The simulation pairs show the maximum and minimum pressures for the simulations with and without heaters. The first simulation in Figure 21 contains a permeability of $1x\ 10^{-11}\ m^2$. The graph illustrates the increase in total pressure when the permeability is reduced by an order of magnitude. The reduction in the permeability increases pressure within the system.

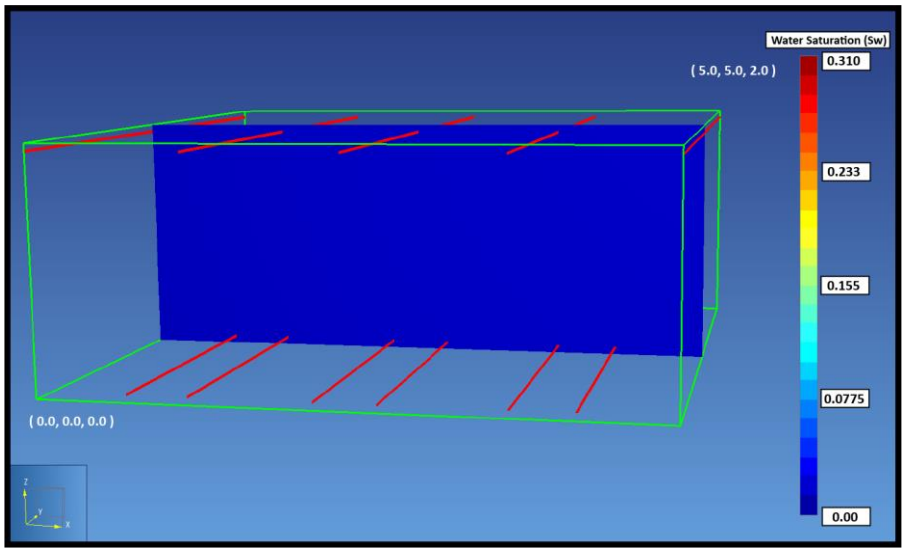

Figure 17: Water saturation (S_w) for the ex-situ base case model at time = 47 days.

The simulations listed in Figure 21 also illustrate the maximum and minimum pressures of the simulation run within out heaters. The constant rate heaters add an additional 1000 Watts to the system and increase the total pressure within the volume. When the heaters are omitted, the maximum and minimum pressures are only slightly lower. Overall the simulations that contain the heaters have higher maximum and minimum pressures.

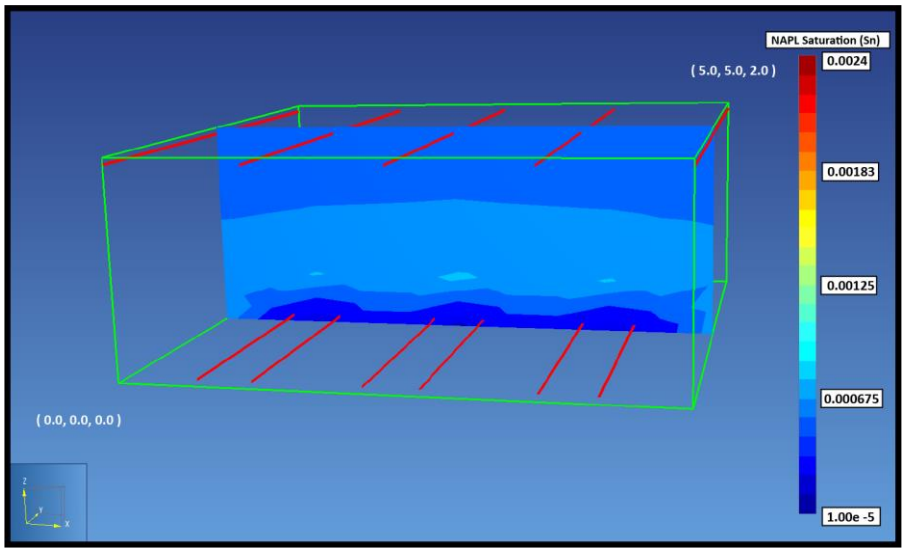

Figure 18: Mercury saturation (S_n) for the ex-situ base case model at time = 8 days. A mercury condensation front appears in line with the base layer injection wells and base layer heaters.

4.5.2 Temperature

The heaters have a greater impact on the removal rate of mercury form the system. The heaters reduce the time it takes for the injected air to heat up the system. If the control volume heats up past the boiling temperature of water the hot air can then vaporize the mercury. This trend is illustrated in Figure 9 where the mass extraction of mercury begins to increase as the water mass approaches zero in the volume. Figure 22 illustrates the faster mercury removal rate when the heaters are present in the base case model. When the base case model reaches a mercury saturation of 1×10^{-5} (98% removal) the temperature within the model is 268°C (Figure 12). When the heaters are omitted form the model the temperature is only 185°C after 58 days of injection (Figure 23). The base case without heaters needed to have air injection for an additional 21 days before all of the mercury was removed.

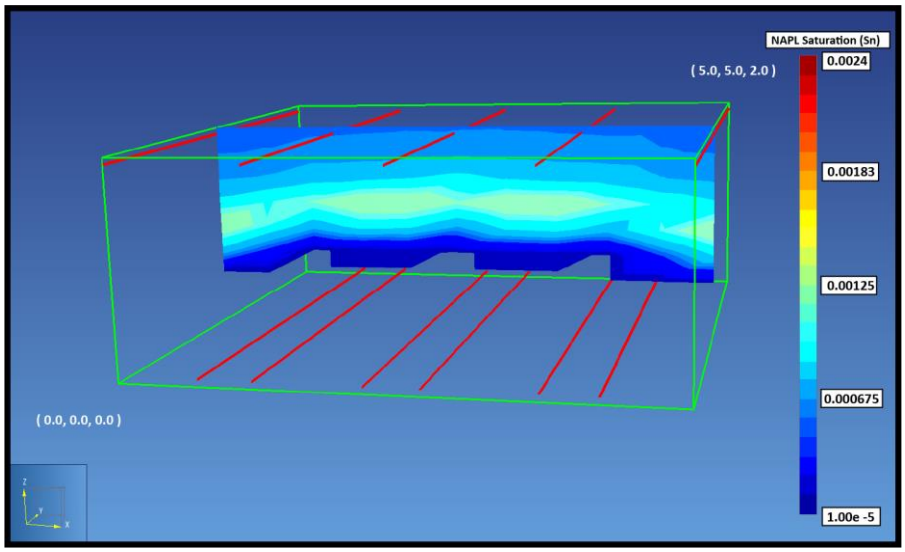

Figure 19: NAPL saturation (S_n) for the ex-situ base case model with no heaters at time = 37 days.

4.5.3 Permeability Comparison

The mercury removal rates are similar in all the permeability cases. The injection rate used to compare the simulation produces a mercury removal time of approximately 60 days (Figure 24). Decreasing the permeability only slightly increases the amount of time necessary to remove the mercury from the system. Figure 24 indicates that the permeabilities are too similar to drastically change the remediation time. If the simulations contained permeabilities varying in values larger than one order of magnitude then the remediation times would be different. The permeabilities used in the comparison are too similar to change the mercury removal times when the simulations are injected with air at the same rate.

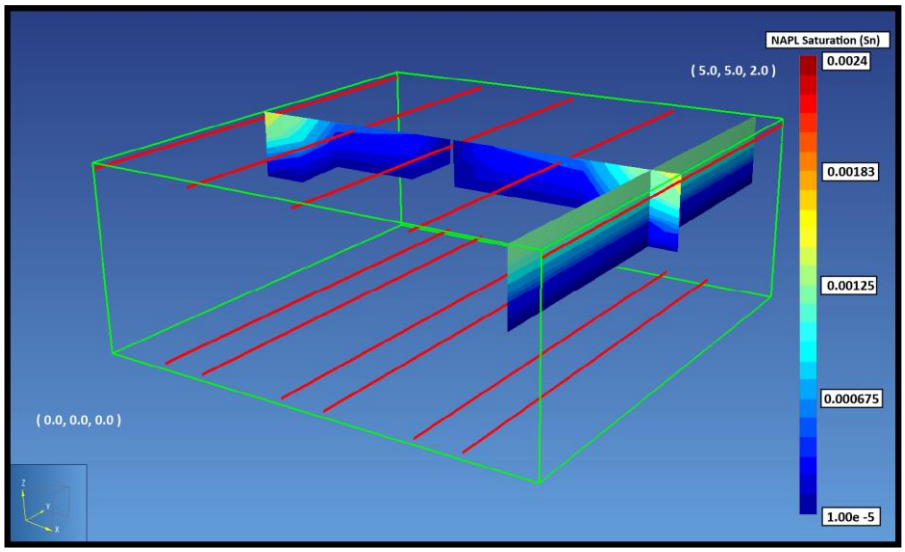

Figure 20: NAPL saturation (S_n) for the ex-situ base case model with no heaters at time = 55 days. An additional slice was added at X = 4.7 m to show mercury condensation in the corners of the model.

A decrease in permeability should restrict the air injection and increases the injection time needed to heat the volume. However, the injection rates are the same in all of the simulations and the removal of mercury is dependent on the rate of air injection. Changes in permeability do not drastically change the mercury removal times but does change the pressure within the volume. The total maximum pressure in each model increases with reduced permeability. It is important to note that the pressure exceeds 3 atm in the low permeability simulation (Figure 21). Simulations run in low permeability soil need to have an adjusted air injection rate to reduce the total pressure. Lower injection rates will reduce the pressure buildup in the low permeability simulations and result longer injection times to remove the mercury.

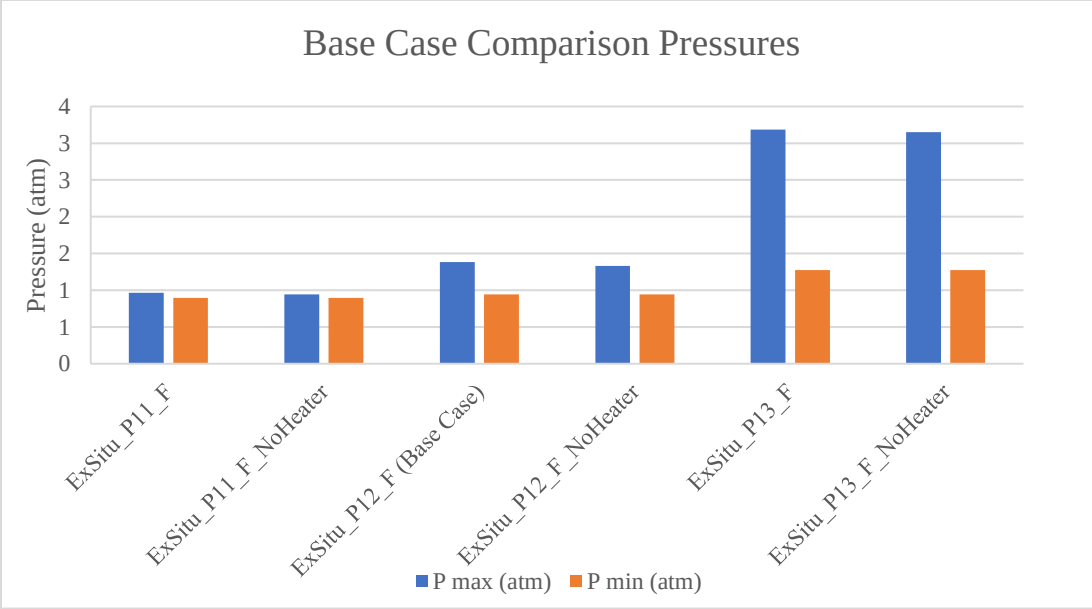

Figure 21: The maximum and minimum pressures of the simulations containing the same injection rate as the base case ex-situ simulation (2.5 x 10^{-3} kg/s (243 L/min) at 300°C) with and without the base layer heaters.

4.6 Conclusion

The energy delivered to the system at a specific rate has proven to be an important variable in early simulations. The rate at which hot air is injected into the system can determine how long it takes to remediate the control volume. However, when the rate of air injection is increased the pressure with the system increases. Precautions must be taken to prevent the internal pressure from getting too high and causing mercury vapors to escape the system A fine balance must be met to prevent the internal pressure from

getting too high while keeping the air injection rate high enough to remove the mercury within a reasonable time.

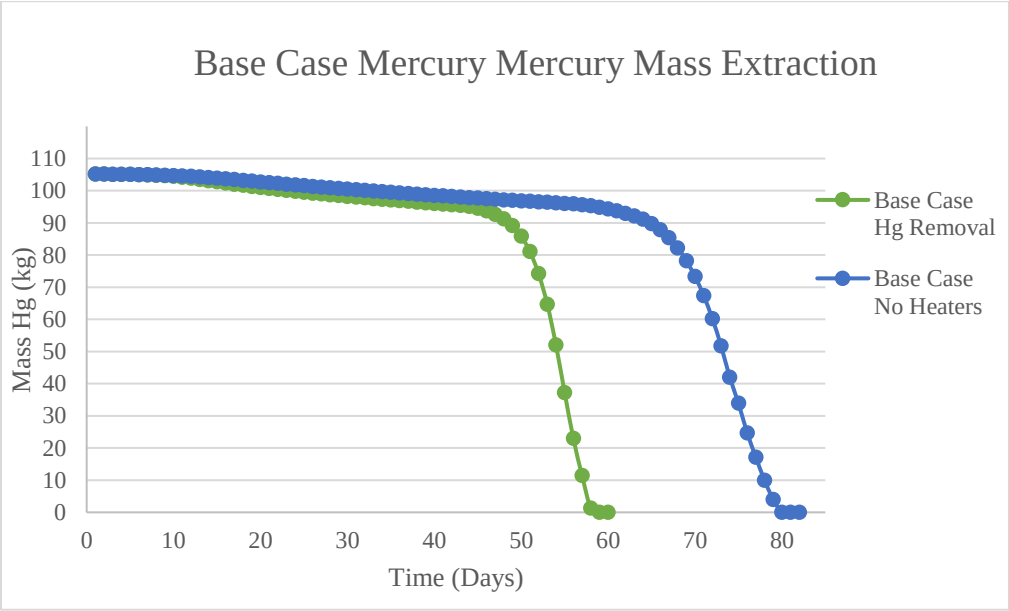

Figure 22: Mercury mass extraction for the base case ex-situ model with and without heaters.

The base case simulation was chosen on loosely defined pressure and application times. The Base Case identification criteria were chosen based on a timely application while keeping the pressure close to atmospheric. It may be more efficient to inject air and water at slower rates in order to reduce the maximum pressure within the system even further. However, for criteria was used to identify an injection rate that could be used to across permeability values. It was expected to see that a decrease in permeability would increase the amount of injection time required to remove mercury from the system. When the permeability of the contaminated material is reduced, the injection rate must also be reduced to accommodate the additional pressure that accumulates within the system.

Based on the simulation comparisons, the presence of heaters at the bottom of the system are not necessary to remove mercury from the system. Although the heaters are

not necessary, they speed up the mercury removal process. In applications where the pressure is not a factor then additional heat can be added to the system. It is important to recognize the design and material of the no flow boundaries constructed to mimic the design of the ex situ thermal treatments options presented in this research. Pressure within the system needs to be addressed and limits set on the maximum pressure the control volume can withstand to prevent the escape of lethal mercury vapor.

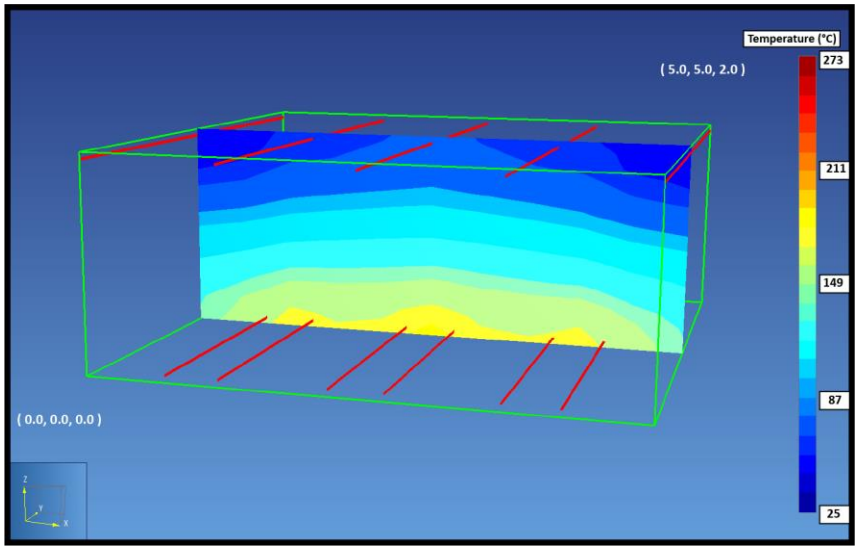

Figure 23: Ex-situ base case model temperature profile after 58 days of injecting hot air at a rate of 2.50 x 10^{-3} kg/s (243 L/min) without the presence of base layer heaters.

The simulations were limited by the critical temperature of water. The simulations are only valid for temperatures below the critical point of water (367°C). This is not an issue as the temperature within the base case model does not exceed 268°C. The heat transfer from the air injected at 300°C is adequate to heat the control volume to 268°C and evaporate mercury at 1 atm of pressure. At lower temperatures mercury has a low vapor pressure (Figure 3) and at 268°C the vapor pressure of mercury is 0.15 atm.

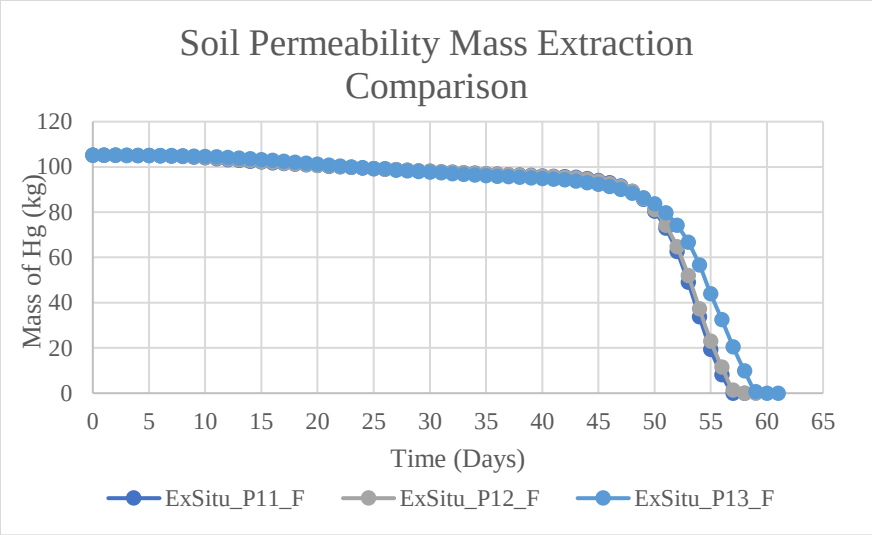

Figure 24: Mercury mass extraction for the ex-situ simulations injected with air at a rate of 2.5 x 10^{-3} kg/s (243 L/min) at 300°C.

Added variables such as soil heterogeneities and multiple species of mercury will make the simulations more realistic and applicable when performing site evaluations. Knowledge and procedures obtained for the model calibration will be integrated into ex-situ model designs that incorporate site information from mercury contaminated sites.

CHAPTER FIVE

IN-SITU MODEL DESIGNS

5.1 Introduction

The research discussed in this chapter involves the development of an in-situ configuration that can be used to remove mercury. Well configurations and the soil capillary pressure were two important variables considered when developing the in-situ method under temperature and pressure constraints. Similar to the ex-situ methods, the in-situ method needs to remove mercury in a timely manner under conditions that minimize the amount of escaping mercury vapor.

5.2 In-situ Model Development

The in-situ model was developed to simulate a portion of soil located in close proximity to the water table. Well geometries were tested in an effort to reduce the amount of pressure localized near the model's surface, at the point of air injection and point of vacuum extraction. In a similar manner to the base case identification in the ex-situ modeling, a base case in-situ model was used to compare various sets of system conditions as well as the effects of a constant injection rate on soil with different permeabilities.

The in-situ model was developed in the following steps: (1) model design (2) establishing initial gravitational equilibrium conditions within the volume, (3) heat and air injection for the mercury removal, and (4) vacuum production for the removal of volatile mercury. The initial conditions within the model were adapted from the ex-situ models described in Chapter 4 but were altered to include features representative of the

in-situ environment. Incorporation of the water table and open boundary conditions are two of the major changes to the model and present unique differences when modeling air injection and mercury vapor extraction. Similar to the ex situ models, air and water mass injection as well as the vacuum extraction rates were varied in order to extract mercury in an effective manner and reduce pressure buildup within the system.

5.3 In-situ Simulations

5.3.1 Design

The in-situ models represent an area of soil contaminated with mercury. The dimensions of the model are 15m x 15m x 15m and it contains 3375 m^3 of unconsolidated sand. The bulk density of 2600 kg/m^3 and porosity of 0.31 remain the same across all the simulations. In the center of the model, a contamination zone contains gas, water and liquid mercury (Figure 25). The contamination zone was represented by the red zone of soil within the model; Figure 26 shows the isolated volume of soil that contains mercury. The system contained 268.8 m^3 of soil contaminated with 566.1 kg of mercury. The overall contamination is high and represent a highly contaminated area with approximately 2 kg of mercury per cubic meter of soil.

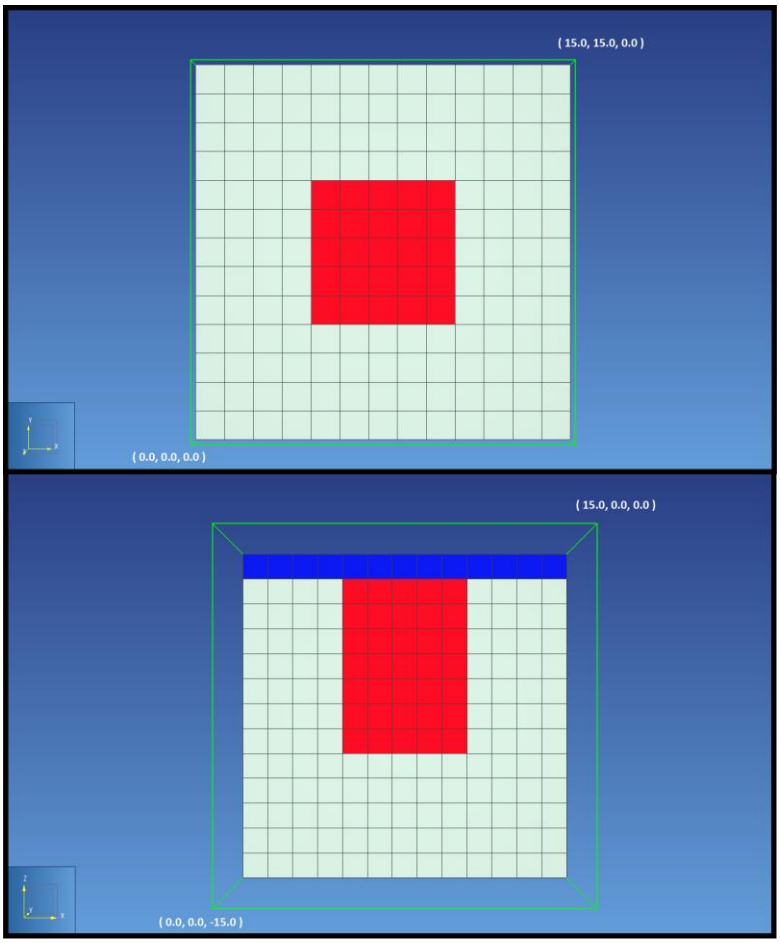

Figure 25: (Top)Top view of the first soil layer in the control volume. The red square represents an area of approximately 33 m^2 and the top layer of the mercury contamination. (Bottom) Cross-sectional view of the control volume. The top blue layer represents the ATMOS, atmospheric layer and red mercury contamination.

The cartesian grid used in the simulations contains 2197 gridblocks. Each gridblock is 1.15 m in length, width and depth and contains 1.54 m^3 of soil. The system is 15 m in length, width and depth and contains 13 gridblocks in each dimension. Decreasing the amount of gridblocks reduced that simulation time. Early simulations had convergence problems when gridblock dimensions were smaller than 1 m^3 resulting in very small timesteps.

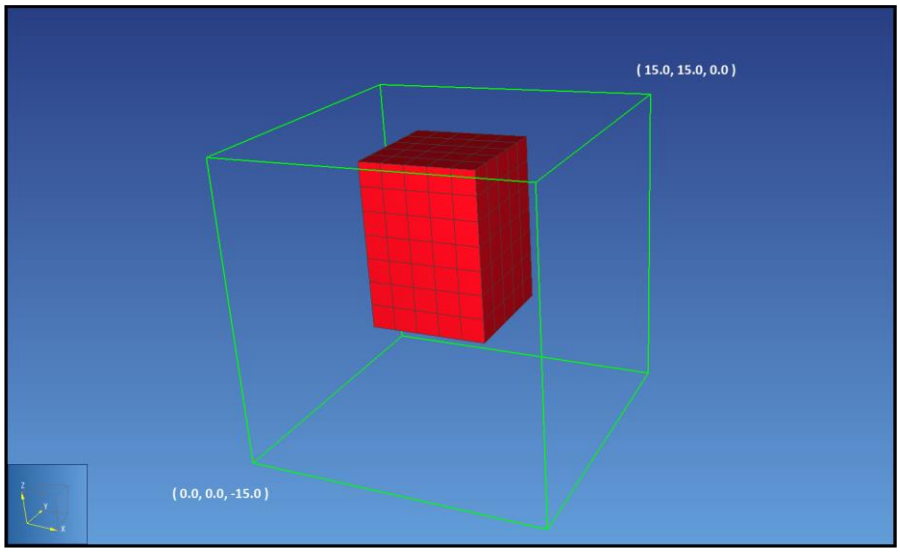

Figure 26: Isolated mercury contamination volume within the in-situ model. The 268.8 m^3 of soil contains approximately 560 kg of mercury.

The gridblocks within the model consist of three types of materials. The materials were constructed to represent atmospheric conditions, soil and soil contaminated with mercury. The materials contained globally defined initial temperature and pressure conditions. The initial pressure was 1.013×10^5 Pa and the temperature was 20°C. The initial phase saturations within the model depend on the capillary pressure used to establish gravitational equilibrium.

The lithostatic stress was calculated in a series of gridblocks that are penetrated by injection and vacuum wells. It was important that the injection of pressures within a gridblock do not exceed the lithostatic stress of the soil. If injection exceeded the lithostatic stress fracture pathways could would propagate within the soil and airflow pathways will be influenced. If airflow deviates around low permeability areas into high permeability areas, such as fractures, large areas of soil can remain contaminated. The lithostatic stress within the system is estimated using

$$P_l = (1 - \emptyset)\rho_R g d$$

Equation 19

where P_l is lithostatic stress; Ø is porosity; ρ_R is the rock grain density; g is the acceleration of gravity; and d is depth from the surface.

The gridblock pressures are recorded in the simulation to make sure that the lithostatic stress of the soil is not exceeded. The pressures within the system need to be reduced to prevent the soil from fracturing and to prevent the possible escape of mercury vapor.

Establishing the boundary conditions (BCs) in the model was important in the in-situ simulations. In TOUGH2/TMVOC the gridblocks can contain fixed temperature, pressures and/or phase saturations. Alternatively, the gridblocks can remain active as time changes within the system where temperature, pressure and phase saturations are calculated according to the partial differential form of the general transport equation. Fixed gridblocks are defined so that the thermodynamic initial conditions within that gridblock do not change with time (Pruess & Battistelli, 2002). The fixed state gridblocks are referred to as Dirichlet boundary conditions and will act as a source/sink for fluid and heat flow (Pruess & Battistelli, 2002). Fixed state gridblocks were essential at the top and bottom of the model when running gravitational equilibrium models (Figure 27). Gravitational equilibrium models allow phase concentrations to settle under the forces of gravity over a time span without the influence of heat or fluids. The gravitational equilibrium model results are loaded into the simulations as initial conditions.

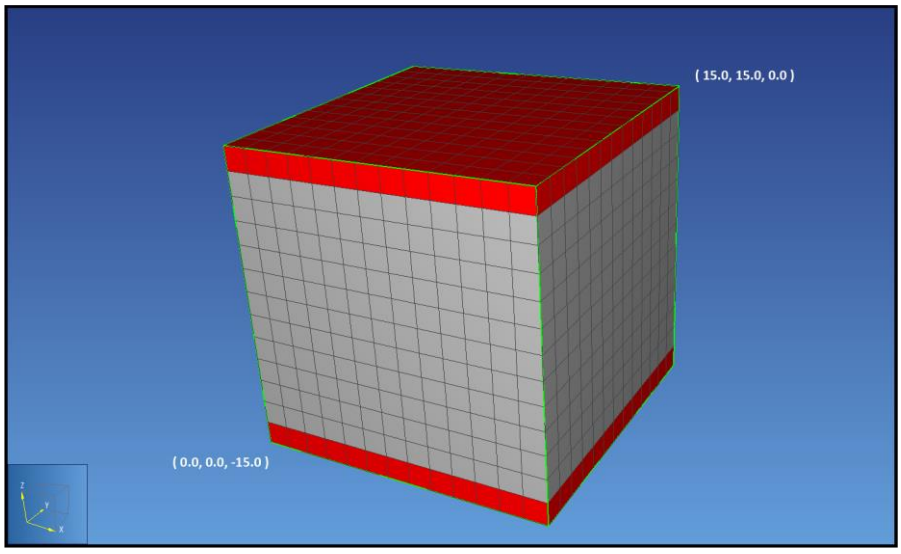

Figure 27: In-situ model geometry illustrating fixed state gridblocks in the top and bottom layers of the model (red gridblocks). The in-situ model geometry with the top and bottom fixed state layers are used to establish 100-year gravitational equilibrium saturations.

Fixed state gridblocks are added to surround the volume when simulating remediation (Figure 28). Surrounding the model in fixed state gridblocks allows temperature, pressure and saturations to remain fixed during the simulation. The fixed state conditions mimic surrounding soil or the atmospheric conditions that would be encountered in the field scale application of thermal treatment with a single well pattern.

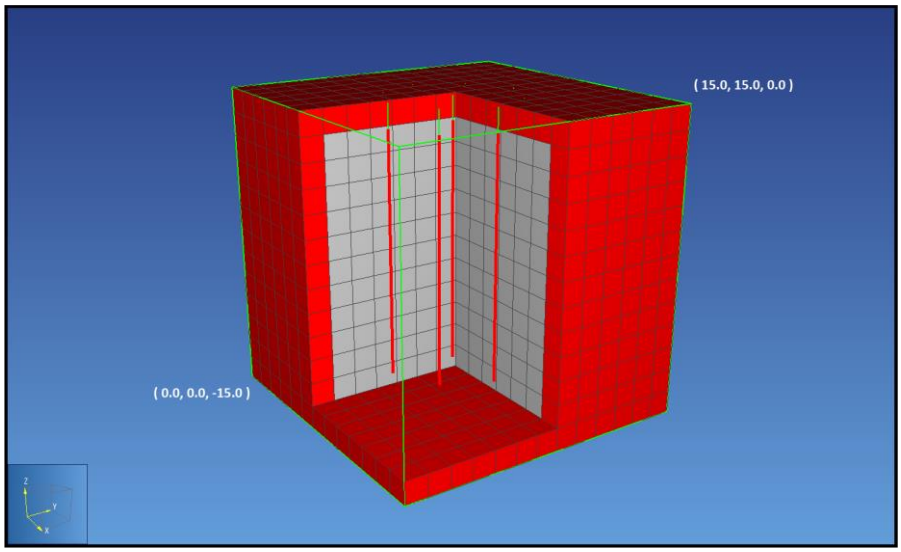

Figure 28: The fixed state gridblocks used to simulate remediation in the in-situ model.

The layer at the top of the model represents the atmospheric conditions and contains water and gas phases. The top layer was designed to contain a moderate permeability of 1.0 X 10^{-15} m². The wet heat conductivity 3.0 W/(m*K) is larger than the dry heat conductivity (1.0 W/(m*K)) as water is a better conductor of heat than air. In addition to the top layer under atmospheric conditions it also acts as a thermal blanket to insulate the remediation area. The low permeability of the top layer is designed to prevent the escape of volatilized water and mercury. The water saturation value (0.099) within the top layer less that the residual saturation (0.1) to prevent spurious water flows into the model. The capillary pressure model was zero for the top layer.

5.3.2 Initial Conditions

The initial conditions within the in-situ model are listed in Table 10. Phase saturations are defined globally for the whole model or locally to define regions based on

the phases present. The area containing mercury contamination contains three phases

In-situ Model Initial Conditions		
Global Water Saturation	0.21	S_w
Global Gas Saturation	0.79	S_g
Top Soil Layer Local Water Saturation	0.20	S_w
Top Soil Layer Local Gas Saturation	0.80	S_g
Bottom Soil Layer Local Water Saturation	0.24	S_w
Bottom Soil Layer Local Gas Saturation	0.76	S_g
Contaminated Soil Top Layer Local Water Saturation	0.201	S_w
Contaminated Soil Top Layer Local Gas Saturation	0.799	S_g
Contaminated Soil Top Layer Local Mercury Saturation	4.94E-04	S_n
Contaminated Soil Local Water Saturaiton	0.201	S_w
Contaminated Soil Local Gas Saturation	0.799	S_g
Contaminated Soil Local Mercury Saturation	4.94E-04	S_n

Table 10: In-situ initial condition saturation values.

(gas, water and mercury) and the rest of the model contained two phases (gas and water). Locally defined water saturations are used to specify the saturations in the second (Atmosphere is the top layer) and bottom layers in the gravitational equilibrium models. Capillary forces draw water into soil and the initial S_w values are calculated based on the distance to the water table. The watertable is assumed to be 1m from the base of the model. The water saturation values for top and bottom soil layers were calculated using the Van Genuchten saturation equation

$$S_w = \left[\left[\frac{P_{cgw}\alpha_{gw}}{\rho_w g}\right]^n + 1\right]^{-m}(1 - S_m) + S_m$$

Equation 20

where water saturation is a function of distance to the water table through the capillary pressure. The center of the gridblocks in the second layer are 14.27 m from the

water table and the center of the base layer gridblocks are 1.58 m from the watertable. Table 11 lists the capillary pressure parameters used to calculate the S_w values in the in-situ simulations. The top and bottom layers of soil contained $S_w = 0.201$ and $S_w = 0.236$. Once the S_w is defined in the top and bottom layers, the remaining saturations are defined at equilibrium.

In-situ Base Case Capillary Pressure Parameters		
Wetting Fluid Saturation Minimum	0.2	S_m
Capillary Pressure Model Exponent	2.5	n
Capillary Fringe Mercury and Gas	10	α_{nw}
Capillary Fringe Mercury and Water	10	α_{ng}

Table 11: In-situ capillary pressure parameters.

Once the influence of the water table has been accounted for and the S_w values have been defined in the top and bottom layers, the remaining soil can be defined as having globally defined saturations as long as the contaminated region has been defined with $S_n = 4.94 \times 10^{-4}$. The amount of mercury contamination within the model was approximately 2 kg/m^3 and $S_n = 4.94 \times 10^{-4}$ for all of the gridblocks that contain mercury

In-situ Base Case Relative Permeability Parameters		
Relative Permeability Water Saturation Residual	0.2	S_{wr}
Relative Permeability Gas Saturation Residual	0.01	S_{gr}
Relative Permeability NAPL Saturation Residual	0.15	S_{nr}
Relative Permeability Model Exponent	2	n

Table 12: In-situ relative permeability parameters.

The residual saturations defined in Table 12 are used to allow water and gas saturations to settle during equilibrium. The gravitational equilibrium simulation will settle the S_w and S_g based on the forces of gravity and the defined phase residuals for the

materials in each gridblock. Since $S_n < S_{nr}$ the mercury is immobile during gravitational equilibrium. When S_{wr}-= 0.20, the majority of the water to falls out of the system. The S_w values in the base layer remain close the locally defined $S_w = 0.236$ after gravitational equilibrium due to capillary forces wicking water up from the water table. Figure 29 indicates the S_w values within the model at distances from the water table. At greater distances form the water table, S_w values remain closer to the S_{wr}.

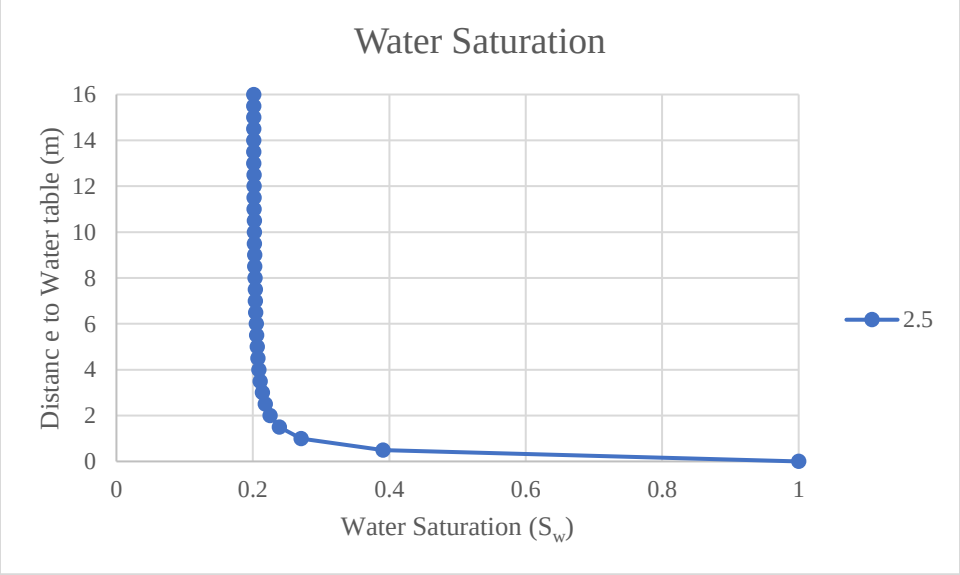

Figure 29: Water saturation (S_w) values calculated using (Parker et al., 1987) three phase estimations and capillary pressure exponent n = 2.5 (Equation 20) and the initial conditions in Table 11.

5.3.3 Wells

Injection and vacuum wells placed in a single well pattern are used to simulate the thermal treatment for mercury (Figure 30). All of the wells used in the in-situ models are screened from the top of the soil (2nd layer from the top) down to 13m. The wells extend deeper into the soil than the extent of the contamination to make sure that heat

is injected beneath the contamination zone.

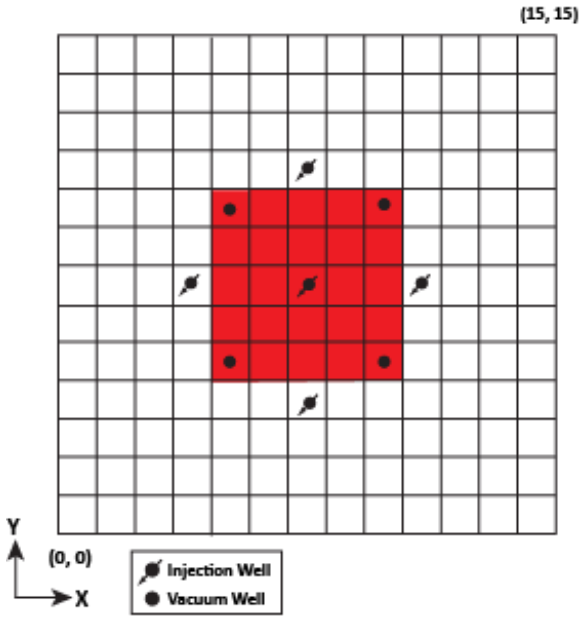

Figure 30: Well configuration used to simulate the in-situ thermal treatment of mercury. The outlined grid represents the top soil layer of the model and is representative of the top area (15m x 15m). The red square represents the top layer of the mercury contaminated area. Four vacuum wells are placed within the contaminated and are placed around injection wells.

Well placement within the volume can alter the effectiveness of the thermal treatment applied to the volume. Drilling and placing wells in a contaminated volume can be costly and displaced borehole cuttings can expose and redistribute contamination. Although the placement of wells can redistribute contamination, a balance needs to be met in order to provide enough air injection to vaporize the contamination and not overload the volume with injection rates exceeding SVE rates. The placement of the injection and vacuum wells controlled the migration of airflow and contamination vapor within the subsurface. Multiple sets of well patterns can prevent lateral migration of contamination away from the sources of heat.

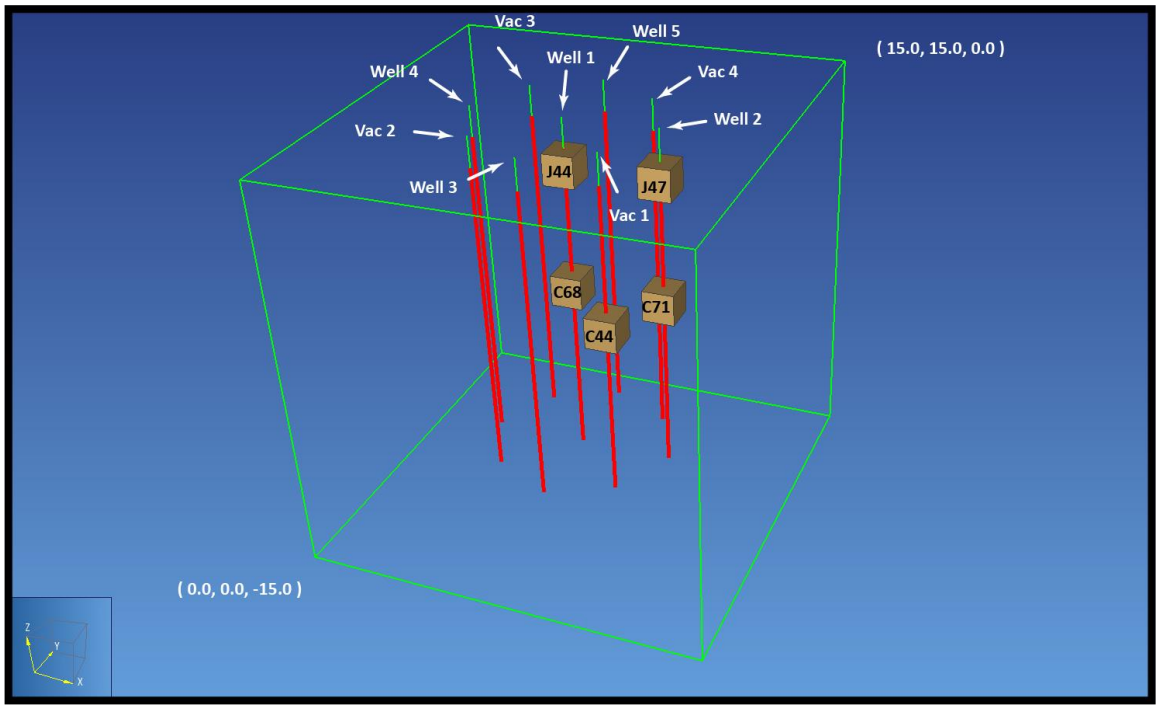

Figure 31: Gridblocks in the first in-situ well geometry used to record injection pressures.

The pressures were recorded in the individual gridblocks shown in Figure 31. The gridblocks were chosen for their proximity to the thermal blanket and location along the wells in the well pattern. Gridblocks J44 and J47 record the pressures along the injection and vacuum wells under the thermal blanket. Gridblocks C68 and C71 record the pressures within the contamination zone in model layer 6. The locations of C68 and C71 were chosen so that the pressures could be recorded in gridblocks that initially contain 3 phases. Gridblock C44 is located along the vacuum well so that the pressures can be recorded adjacent to the central and proximal injection wells.

Pressure buildup occurs underneath the three-phase contamination zone as air is injected. The lithostatic stress for each to these gridblocks were calculated and to see if injection pressures exceeded the forces exerted on the soil from the overburden. Air

injection was varied within the model to simulate the removal of mercury. Injection rates varied from 1.25 x 10^{-2} to 3.0 x 10^{-1} kg/s with the 1/50th fraction of vapor water to account for humidity. The rates of injection were needed to provide adequate amount of heat to remove the mercury from the volume. The mercury mass extraction ranged from 5 years to 20 days depending on the injection rate. The shorter cleanup times are associated with higher injection rates and gridblock pressures Injection times longer than two months could be less cost effective, although longer injection times reduce gridblock pressures. The maximum injection pressure in gridblock (722) must not exceed the 2.5 atm lithostatic stress to avoid possible fracturing.

5.4 In-situ Base Case Simulation Results

The in-situ base case simulation was chosen in the same manner as the ex-situ base case and was chosen to track the effects on the remediation on soils with varying permeability.

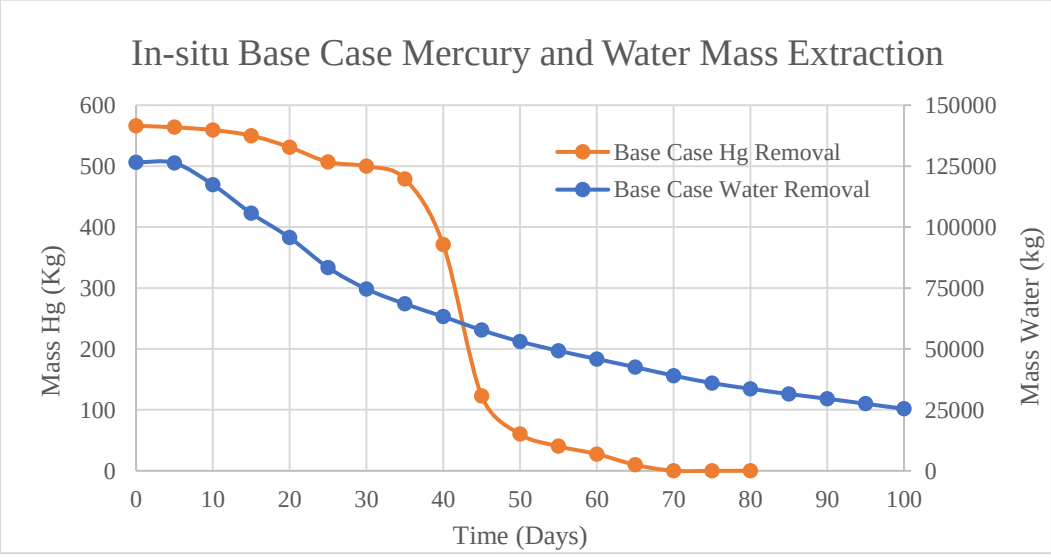

Figure 32: Mass extraction for in-situ base case model. The mercury mass extraction is plotted on the left vertical axis and the water mass extraction on the right.

The middle case soil permeability of 1 x 10^{-12} m^2 was raised and lowered by an order of magnitude to record the effects of soil permeability on the model.

Figure 32 indicates the mass of water and mass of mercury removed in the whole volume. Since the mercury contamination zone represents 268.8 $m^3$of the total 3375 m^3 removing all of the porewater from the volume is not necessary for the removal of mercury. Only the porewater within the contaminated region needs to boil off before mercury can be extracted. Cell J32 is located between wells #1 and Vac #2 and within the mercury contamination zone. Mass extractions were shown for the mass of water and mercury removed from cell J32 (Figure 33).

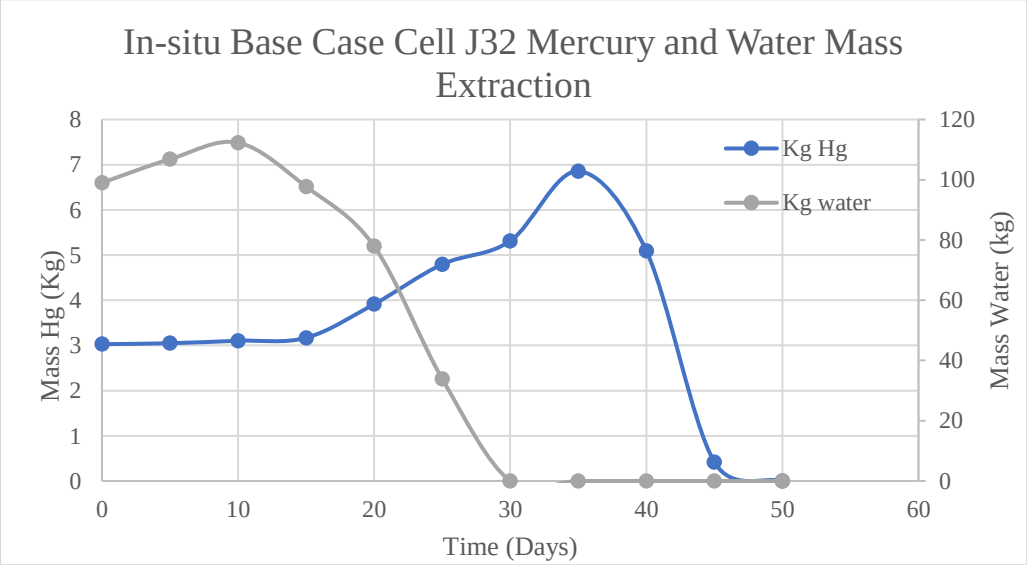

Figure 33: Mercury and water mass extraction from cell J32. Cell J32 is located between well #1 and vacuum #2 in the top layer underneath the thermal blanket. J32 was used to record the amount of water removed from the contamination zone before mercury can evaporate.

Temperature in the base case simulation heats up from an initial temperature of 20°C. Figure 34 shows the max temperature after 5 days of injecting air at 1.0 x 10^{-1} kg/s

(9727.5 L/min) with an enthalpy of 3.01 x 10^5 J/kg. After 50 days of injection the heat

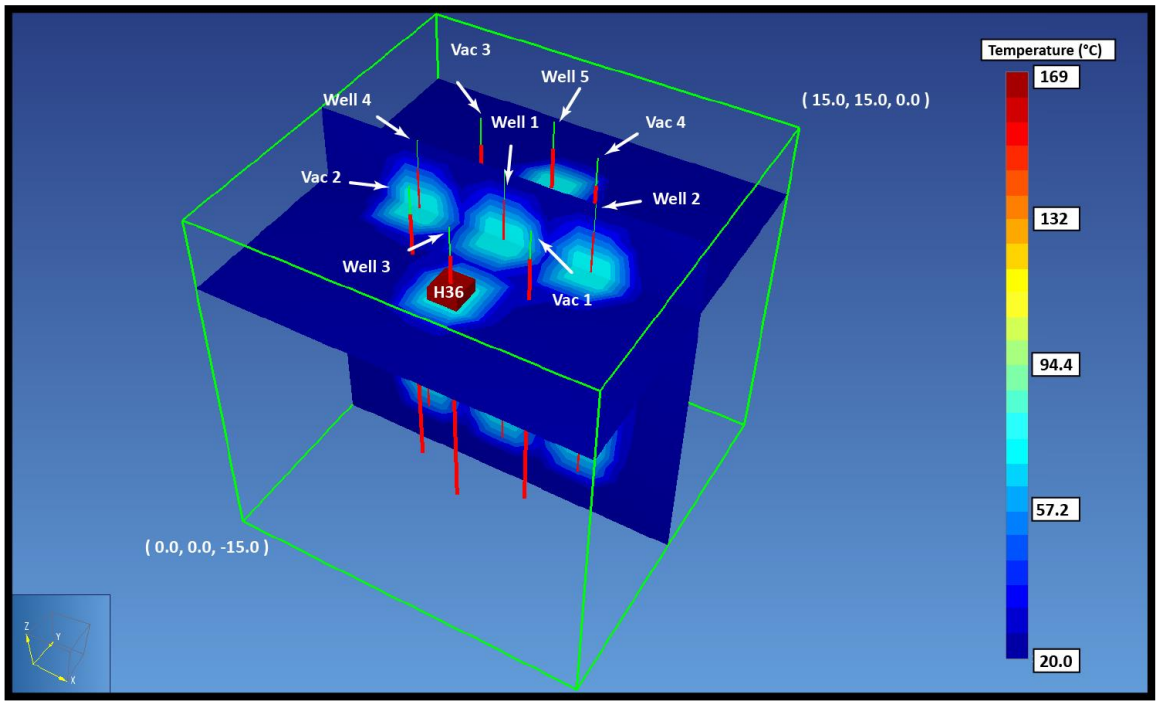

Figure 34: Temperatures for the in-situ base case model at time = 5 days. An additional slice plane at Z = -2.88m shows gridblock H36 which was used to record injection temperatures.

delivered to the system is sufficient to boil porewater and vaporize mercury so the Sn ≤ 1 x 10^{-5} (Figure 35). The temperature scale in Figure 36 indicates the maximum temperature did not exceed the temperature of the injected air. After 50 days, temperatures reached 262 °C in gridblock H36.

Pressures within the control volume were recorded at the timestep where the mercury saturations are reduced below 1 x 10^{-5} (98% removal). The majority of the

mercury was removed from the volume at the end of each simulation. However, a small residual fraction of mercury remained in the volume.

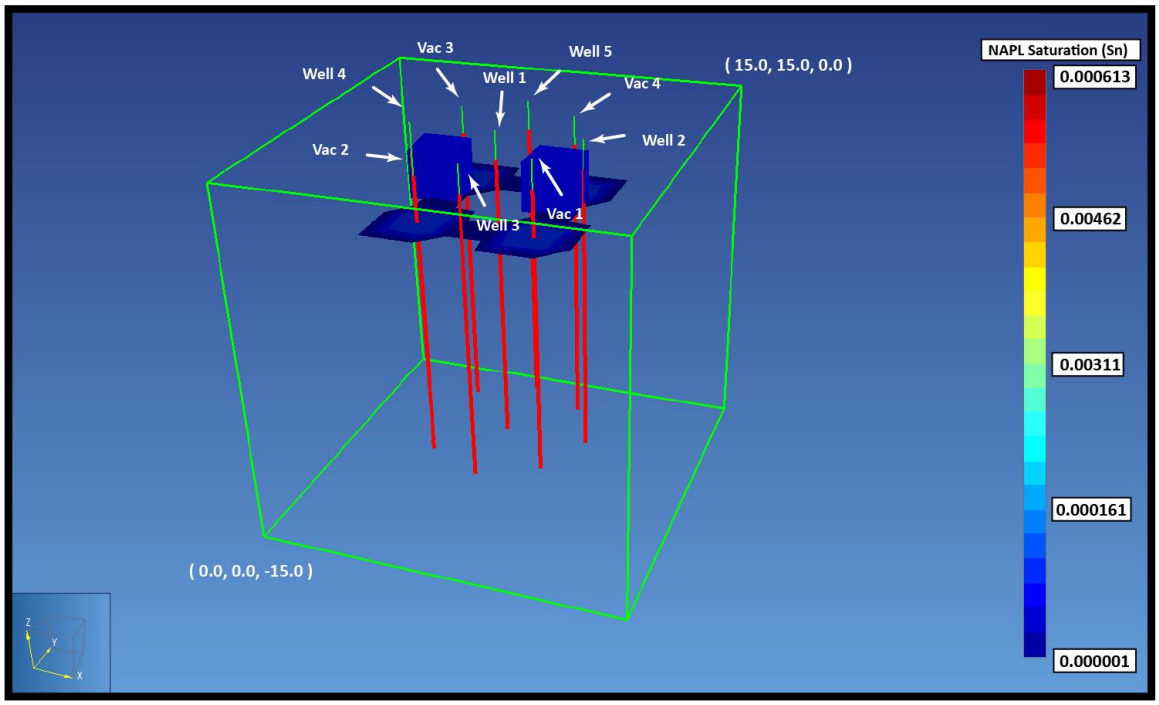

Figure 35: Mercury saturation (S_n) for the in-situ base case model at time = 50 days. After 50 days of injection $S_n \leq 1 \times 10^{-5}$. A small amount of mercury condenses around the extraction wells and underneath the thermal blanket

The water and NAPL saturation fronts are similar in the in-situ simulations and follow the general trend explained in the ex-situ simulations. The injection of hot air and water are used to heat up the volume, boil off pore water, then evaporate mercury. Porewater must first boil at 100 °C so that the local temperature raised above the boiling temperature. Figure 37 illustrates the removal of porewater after 5 days of injection. The water was reduced at a fast rate with limited accumulation and condensation in the areas

outside the heaters (Figure 38). Figure 39 shows that after 50 days of injection the porewater is mostly removed.

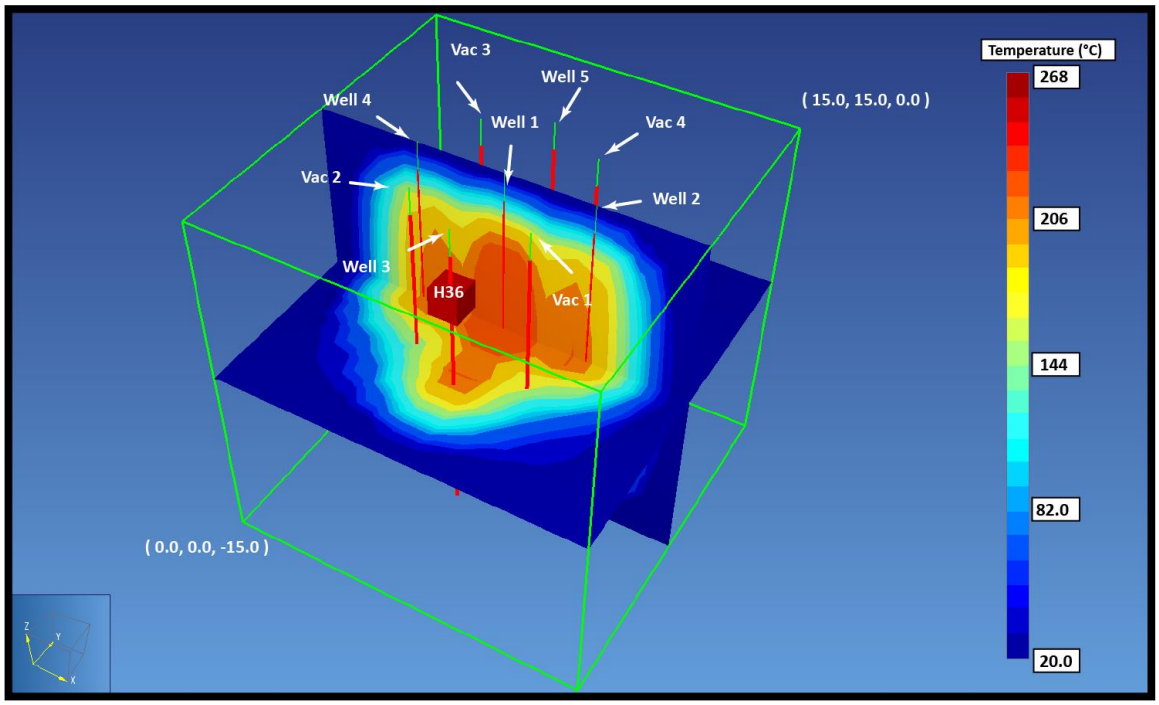

Figure 36: Temperatures for the in-situ base case model at time = 50 days. The temperature recorded in gridblock H36 is 262°C. Slice planes are located at Y = 7.5m and Z = -7.0 m.

The mercury saturation follows a similar trend to the water saturation. After 5 days of air injection, mercury saturations start to increase within the control volume (Figure 40). The saturation scale indicates that the condensation of vaporized mercury increases to S_n values larger than the initial 4.94 $x10^{-4}$ after 5 days of injection. After 50 days of injection the Sn values drop below 1 x 10^{-5} in some locations but the overall mercury mass removed is 60.22 kg (89%) A small amount of mercury remains surrounding the extraction wells and under the thermal blanket. Within 5 days all of the

S_n values are below 1 x 10^{-5}. After the next 20 days of injection all of the mercury was removed from the system for a total of 65 days of injection.

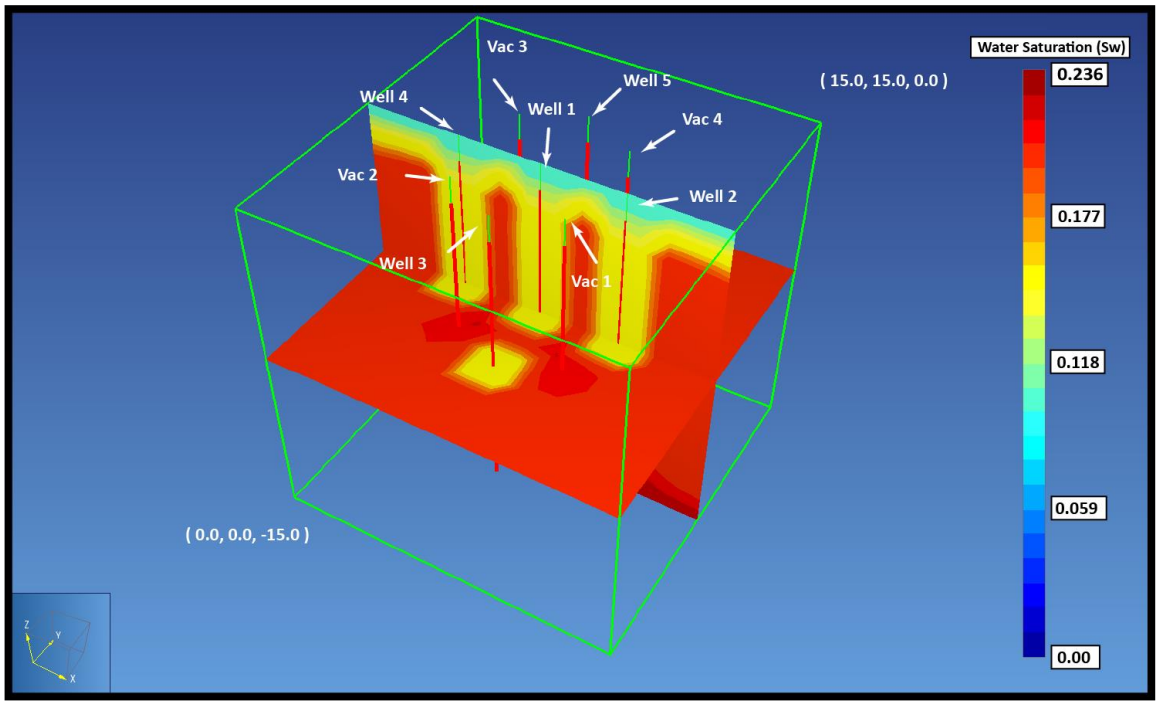

Figure 37: Water Saturations (S_w) for the in-situ base case model at time = 5 days. The slice plane at Z = 7.0 m shows lateral mercury condensation in the corners of the model.

5.5 In-situ Discussion

Well configurations and capillary pressure are two of the variables discussed in this section. The placement of injection wells needs to contain a contamination zone and prevent the lateral movement of phases beyond the heat zone. The simulations sensitivities to the capillary pressure and the relative water permeability were identified when reducing total gridblock pressure.

Moderate Injection rates may be required to lower the total pressures within the gridblocks. However, lower injection rates are not sufficient enough to remove mercury

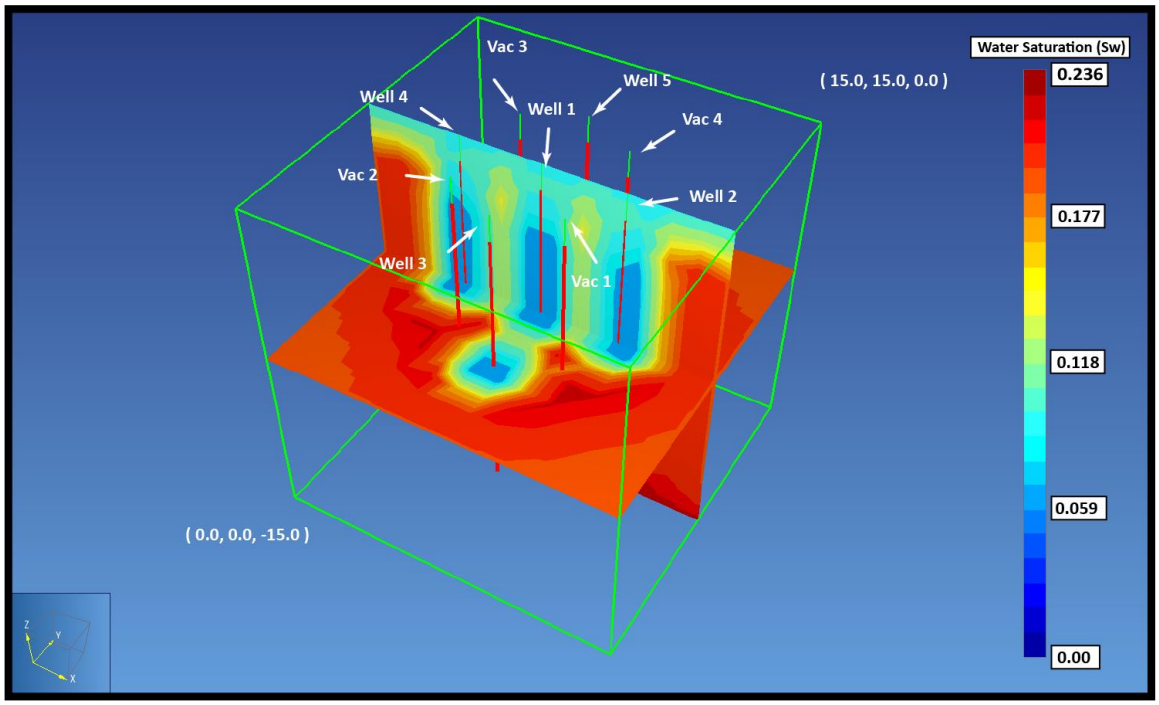

Figure 38: Water Saturations (S_w) for the in-situ base case model at time = 10 days. The slice plane at Z = 7.0 m shows lateral water condensation as air is injected into the model.

in a timely manner. Lower injection rates need to be maintained for longer amounts of time in order for mercury to be removed.

5.5.1 In-situ Wells

Well placement and air injection need to surround the mercury contamination area with heat. The injected air heats up the soil in a circular pattern around the well due to convection. Areas between the injection wells are not subjected to heat if the permeability restricts the airflow between the injection wells. The reduced airflow between the injection wells can leave the cool areas adjacent to the wells with contamination.

Injection wells surround the contamination zone and inject heat into the volume on four

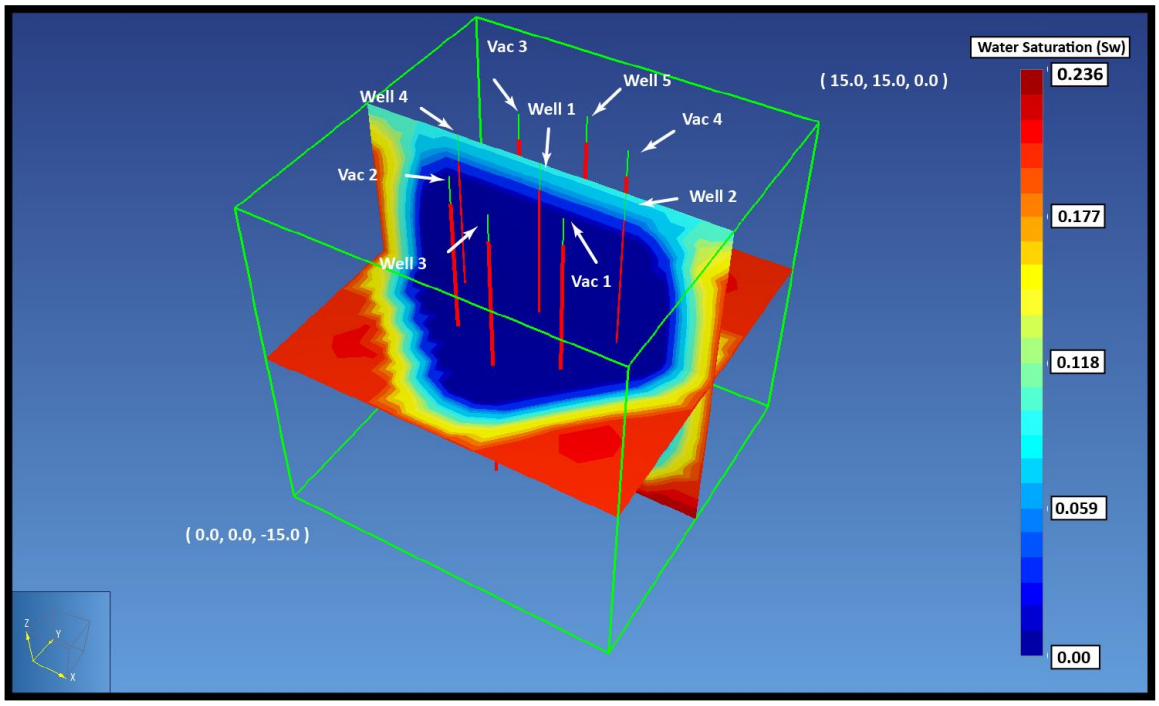

Figure 39: Water Saturations (S_w) for the in-situ base case model at time = 50 days. The slice plane at Z = 7.0 m shows lateral water condensation in the corners of the model.

sides. Increasing the injection rate can expose more soil to heat but increases the risk of fracturing when total pressures approach the lithostatic stress. In addition to fracturing, over injection can occur when the injection rate is increased, A high permeability sensitivity was discovered when the cold areas between the injection wells remain contaminated with mercury. Additional wells were added to the high permeability case to prevent the cool regions from remaining contaminated.

5.5.2 In-situ Relative Permeability

Adjustments to the relative permeability model were made to vary the mobility of the phases within the volume. The relative permeability is a soil property that cannot be altered to increase the mobility of the phases present. However, sensitivities discovered

from altering the model can help identify the conditions where phases are

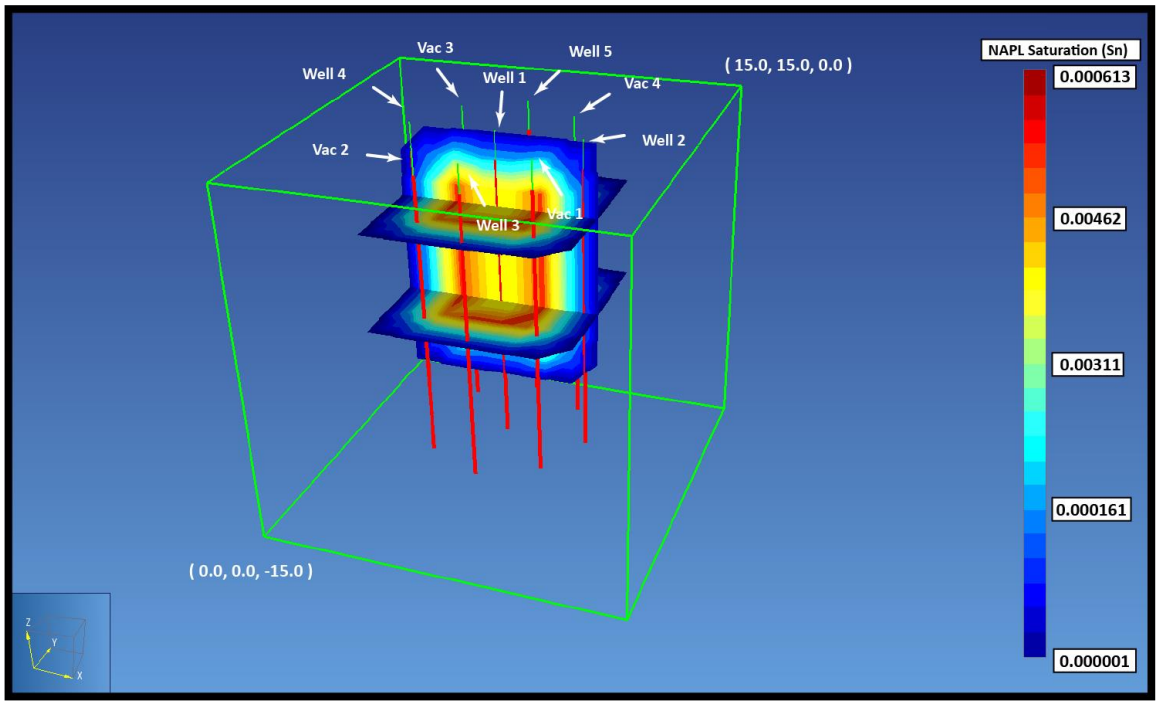

Figure 40: Mercury saturation (S_n) for the in-situ base case model at time = 5 days. The S_n scale indicates values larger than the initial $S_n \leq 4.94 \times 10^{-4}$ After 5 days of air injection, mercury saturations start to condensate. Slice planes at Z = -3.0 m and Z = -7.0 m to illustrate the lateral extent of the contamination plume.

mobile. Assigning the value of n = 2 in Equation 16 increased the relative water permeability. Figure 41 indicates that when the relative permeability exponent (n) is reduced from 3 to 2 the relative permeability of the water increases for a specific saturation. Decreasing the relative permeability exponent (n) then increases the flow of water while the flow of mercury and gas remains the same. Increasing the flow of water decreases the amount of time needed to evaporate and remove water from the volume.

5.5.3 In-situ Capillary Pressure Model

Adjustments to the capillary pressure model exponent (n) in Equation 14 increased the mass removal rate of mercury. Figure 42 illustrates the mercury mass

extraction rates with air injection at 1.00 x 10^{-1} kg/s across two sets of initial conditions

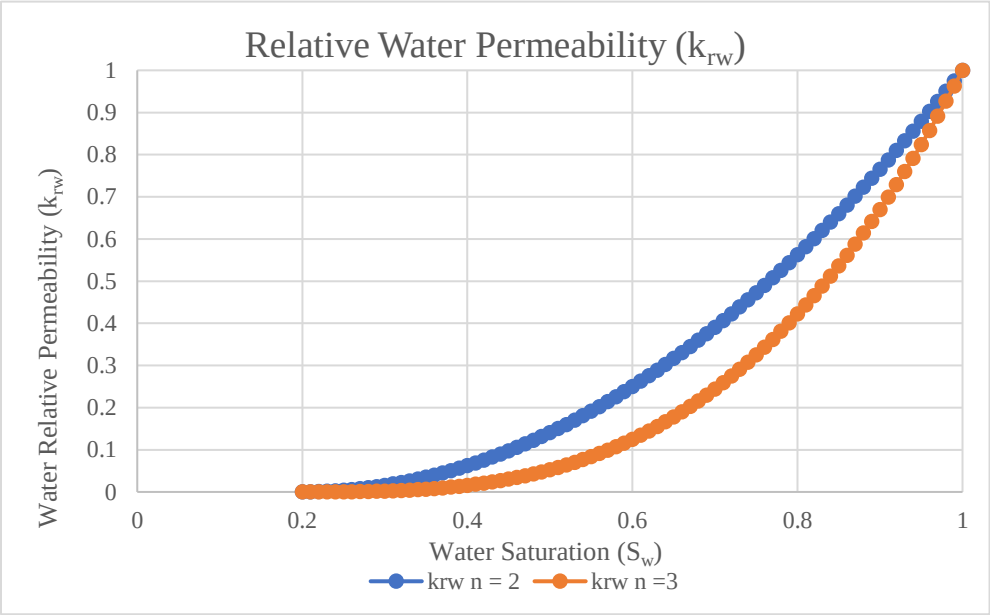

Figure 41 Relative permeabiliy water saturation curves showing the water retention using exponents 2 and 3 (Equation 16).

with different capillary pressure exponents. Increasing the capillary pressure model exponent (n) from 1.5 to 2.5 in Equation 14 reduced the amount of injection time needed

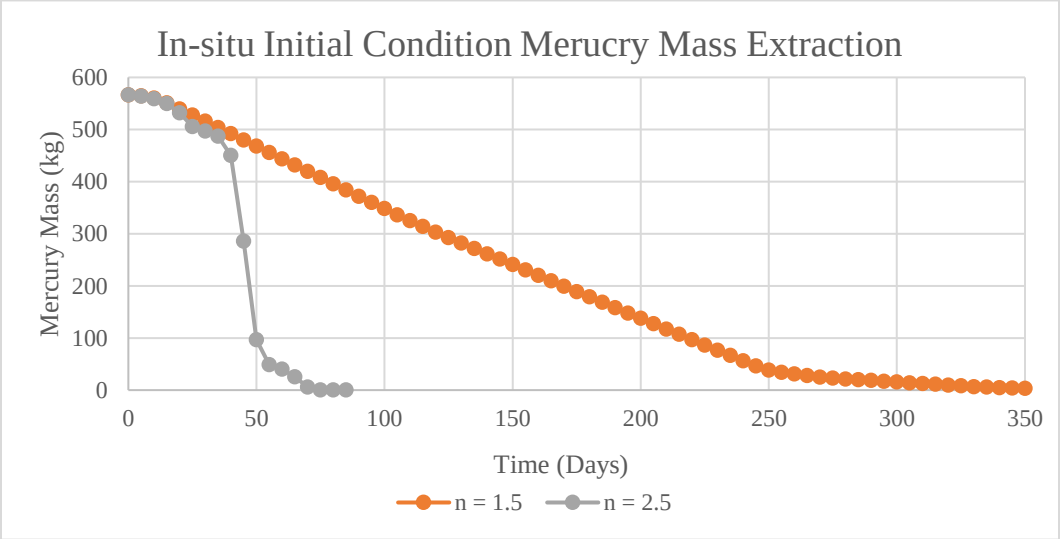

Figure 42: Mercury mass removal comparison models containing 1.00 x 10^{-1} kg/s air injection and capillary pressure exponents n = 1.5 and n = 2.5 (Equation 14).

to remove mercury. Figure 43 indicates that increasing the value of n from 1.5 to 2.5 reduces the amount of water the volume can hold at a given capillary pressure in relation to the S_{wr}.

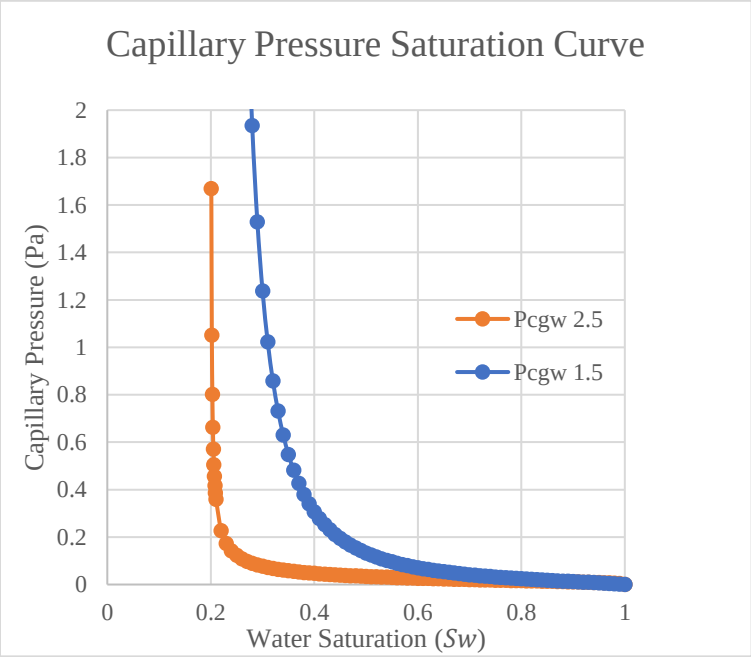

Figure 43: Capillary pressure and water sautration (S_w) curve based on Parker's three phase estimations (Equation 14) (Parker et al., 1987).

Changing n from 1.5 to 2.5 changed the initial saturations defined using Equation 20 in the equilibrium simulations. Figure 29 indicates the S_w values used to establish equilibrium when n = 2.5 remain much closer to the S_{wr} = 0.2 and indicate that less water distributes in the volume during equilibrium. Figure 44 indicates the S_w values are higher when n = 1.5 and the model retains more water. When saturations are higher at a given capillary pressure, the model can retain more water. Water can wick up from the water table as porewater evaporates and draws a vacuum.

5.5.4 In-situ Permeability Comparison

The base case ex-situ simulation contains a permeability of 1 x 10^{-12} m^2 and represents the medium permeability case. Higher and lower permeability simulations are used to compare the effects soil permeability has on time for mercury. The same air injection rates are used in the simulations to provide information on how pressure and cleanup time is altered as hot air flows through soil with varying permeability. Air was injected at a rate of 1.00 x 10^{-1} kg/s and water was injected at 1/50th the ratio to account for the humidity in the air.

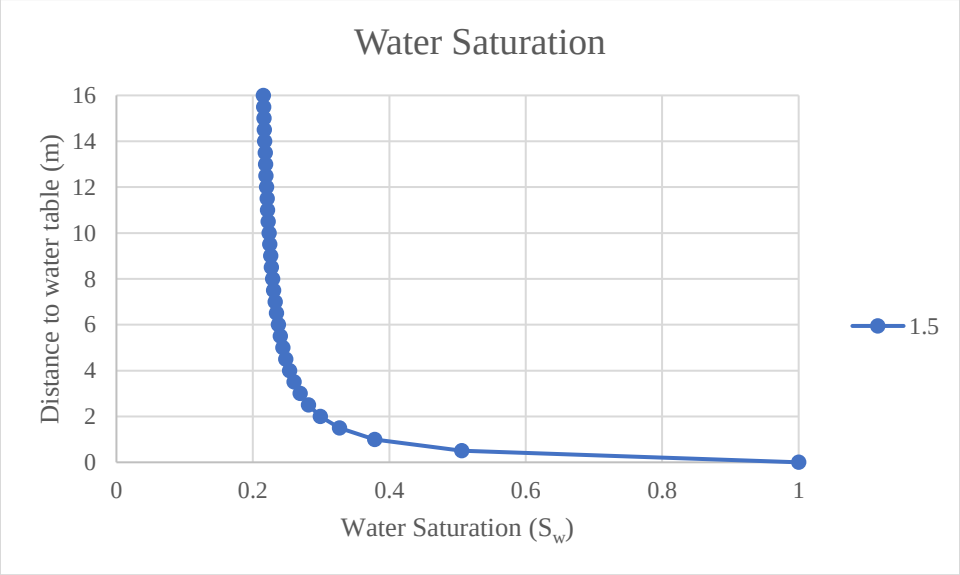

Figure 44: Water saturation (Sw) values calculated using (Parker et al., 1987) three phase estimations and capillary pressure exponent n = 1.5 (Equation 20).

The pressure graphs illustrated in Figure 45 indicate the total pressures and lithostatic stress. The simulation containing the largest soil permeability (1 x 10^{-11} m^2) recorded the lowest pressures. The injection pressure recorded in gridblock J44 is important to track as it is the pressure that builds up below the thermal blanket. Pressures underneath the thermal blanket need to be managed in order to prevent mercury vapor from escaping the system. Pressure buildup is expected to be larger in lower permeability

soils. Airflow within low permeability soil is reduced and this is expected in heterogeneous soils.

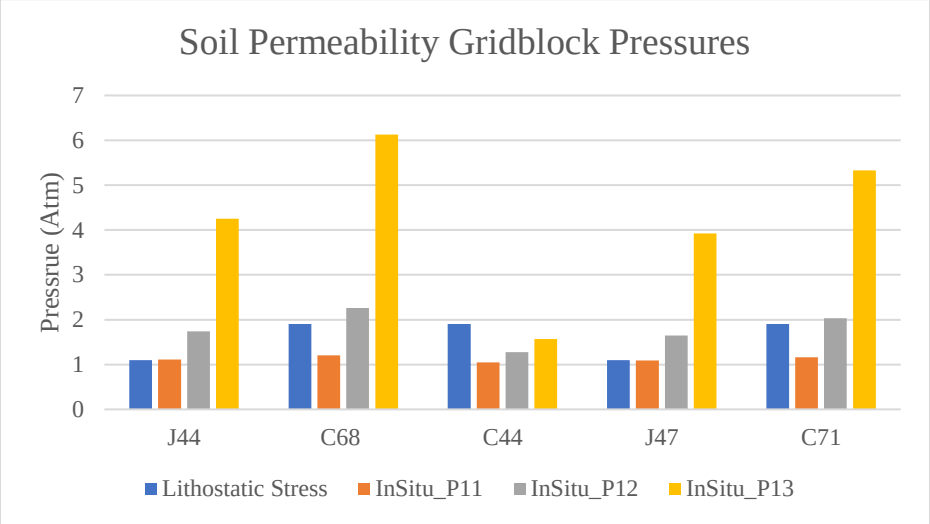

Figure 45: In-situ soil permeability gridblock pressures.

The mercury mass extractions were compared to the simulations containing the same injection rates (Figure 46).

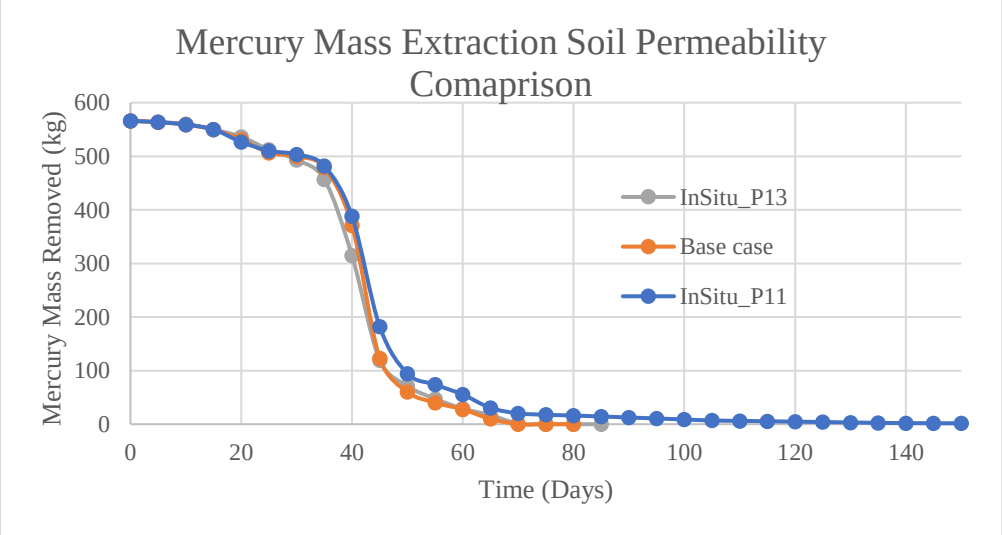

Figure 46: In-situ mercury mass extraction soil permeability comparison.

The base case in-situ model contains a mercury mass extraction rate similar to the higher and lower permeability models. The major difference is the large asymptotic tail that occurs in mass extraction in the high permeability simulation. The removal time indicates a fraction of mercury that resides in volume. The three-dimensional results for simulation high permeability case indicate that after S_n falls below 1 x 10^{-5} a small amount of mercury collects in the corners of the control volume (Figure 47). The high permeability simulation takes greater than 200 days to remove mercury below 0.10 kg within the system, a total of 55 additional days of injecting air at a higher rate than 5.00 x 10-2 kg/s.

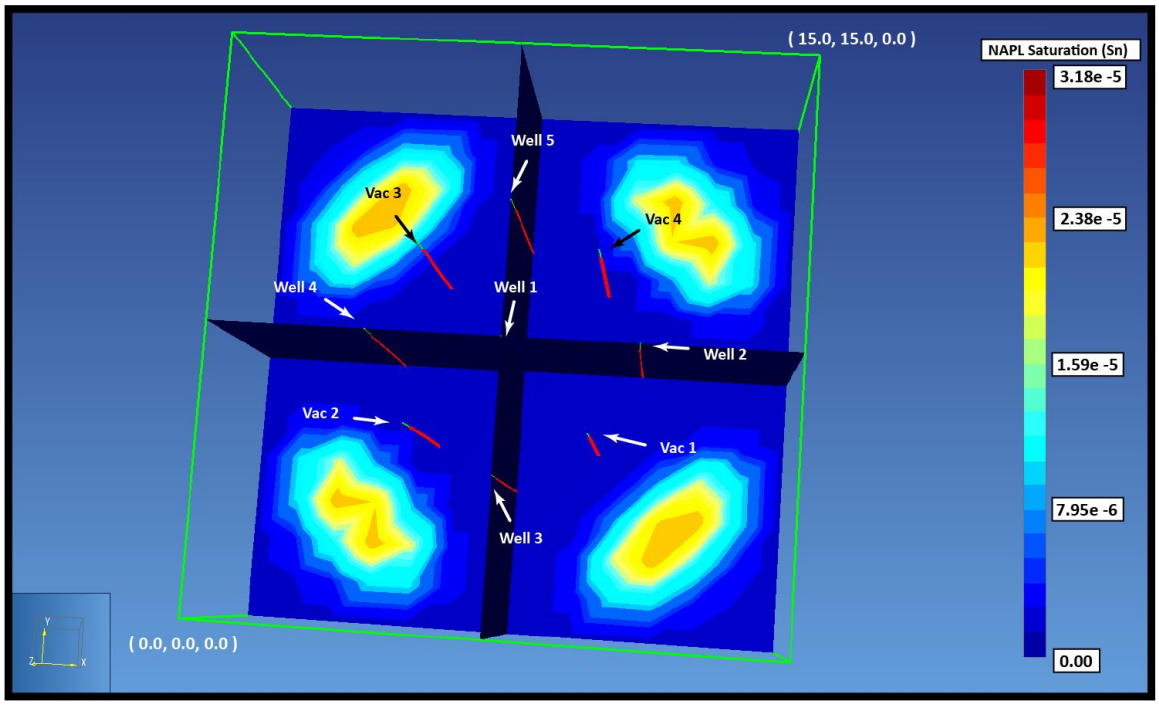

Figure 47: Mercury saturation (Sn) for the higher permeability in-situ model at time = 70 days. The Sn scale indicates saturations ranging from 0.00 to 3.18 x 10^{-5}. The saturation is well below the saturation of 1.00 x 10^{-5} used to record the pressure values. The residual mercury condenses along the fringe of the heat zone.

The in-situ simulations with injection rates higher than 1.00 x 10-3 kg/s take longer for the residual mercury to be removed from the system and indicates a small amount of mercury that has condensed on the outer fringe of the heat zone. Higher air injection rates

can push mercury vapor outwards when the injection rate well pattern exceeds the extraction rate. The higher permeability case is over injected by approximately 2.00×10^8 kg of air and pushes mercury contamination outside the region of hot air. The rate of injection needs to be less than or equal to rate of extraction in order to prevent mercury from collecting in the cooler, outer fringe of the model. The vacuum rates within TOUGH2/TMVOC are limited pressures less than atmospheric. Addition wells are need to provide larger extraction rates in the simulations and to prevent over-injection.

Altering the permeability of the soil by one higher and one lower order of magnitude does not drastically alter the mercury mass extraction. Mercury mass extraction is dependent on the evaporation rate of water and the amount of water within the model does not change in each of the varied permeability cases. However, the reduction in permeability reduces the amount of airflow pathways that promote the migration of contamination. In order to prevent the residual mercury from residing in the control volume additional injection wells were added to surround the contaminated volume. Increasing the number of vacuum wells, or increasing the rate of extraction in could decrease the chance of over injecting the volume. However, pressure constraints in TOUGH2/TMVOC limit the amount of negative pressure applied by a vacuum well. For this reason, it is easier to place additional injection wells in the model in an effort to reduce the migration of contamination out of the heating zone.

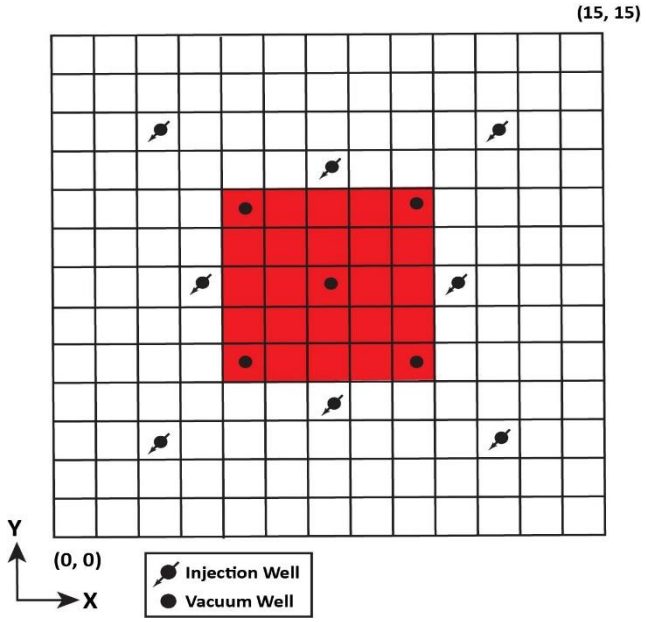

Figure 48: Additional well geometry used to contain the mercury contamination area with injection wells. Additional wells are added to surround the mercury contamination zone with heat from injection wells.

Four additional injection wells are were used to surround the contaminated area with heat (Figure 48). The additional injection wells were only used to see if residual mercury remained in the corners of the volume after approximately 65 days of injection. Adding injection wells increases the likelihood of over-injection, but the wells were added only to show that surrounding the contamination zone in heat can prevent the lateral migration of contamination. Additional vacuum wells are needed to prevent over-injection but were omitted for the lack of ability to increase the negative pressure beyond atmospheric. Figure 49 illustrates the influence of the additional injection wells after 25 days of injection.

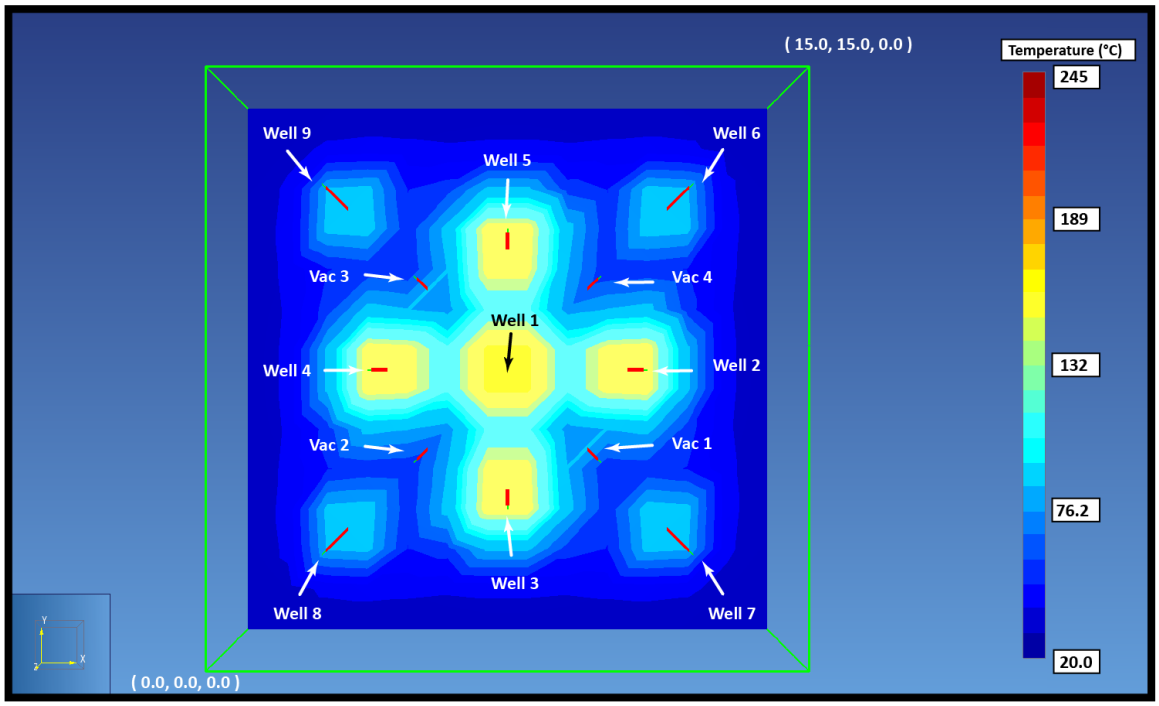

Figure 49: Temperature for the in-situ base case model at time = 25 days. additional air is used to contain lateral mercury migration and to prevent residual mercury from remaining within the control volume.

The mercury mass extraction was graphed for the higher permeability case with additional wells in Figure 50. The additional wells surround the mercury contamination and residual mercury from residing in the volume. The wells were added to the in-situ simulations containing soil with a permeability of 1.00×10^{-11} m^2 and the same air injection rate as the base case. The pressures within the higher permeability case with additional wells simulation was recorded and plotted in Figure 51.

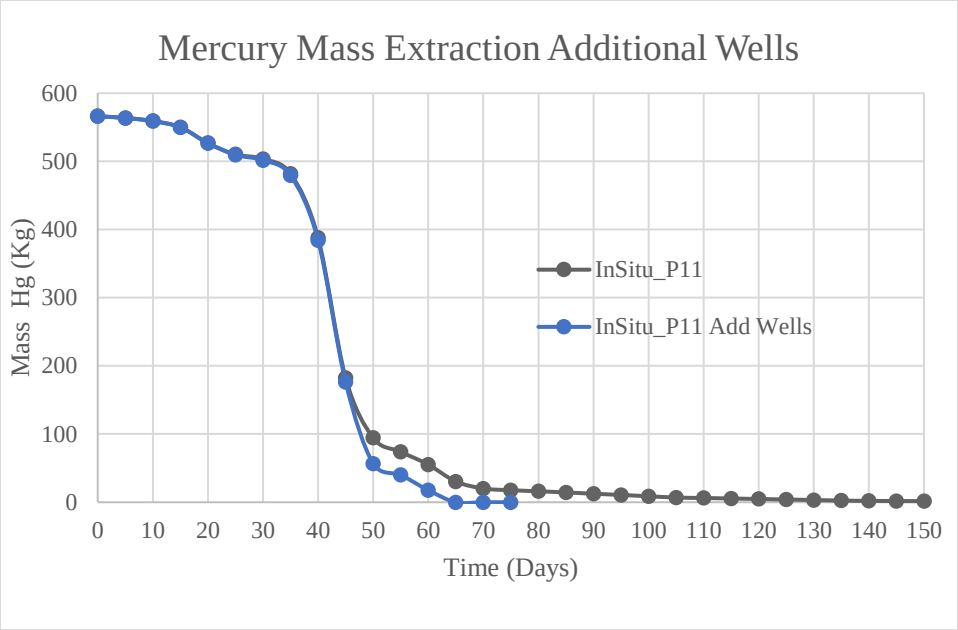

Figure 50 Mercury mass extraction in the higher permeability case and the effect of additional injection wells on simulation.

The pressure values in the higher permeability case with additional wells remain below the lithostatic stress of the gridblocks.

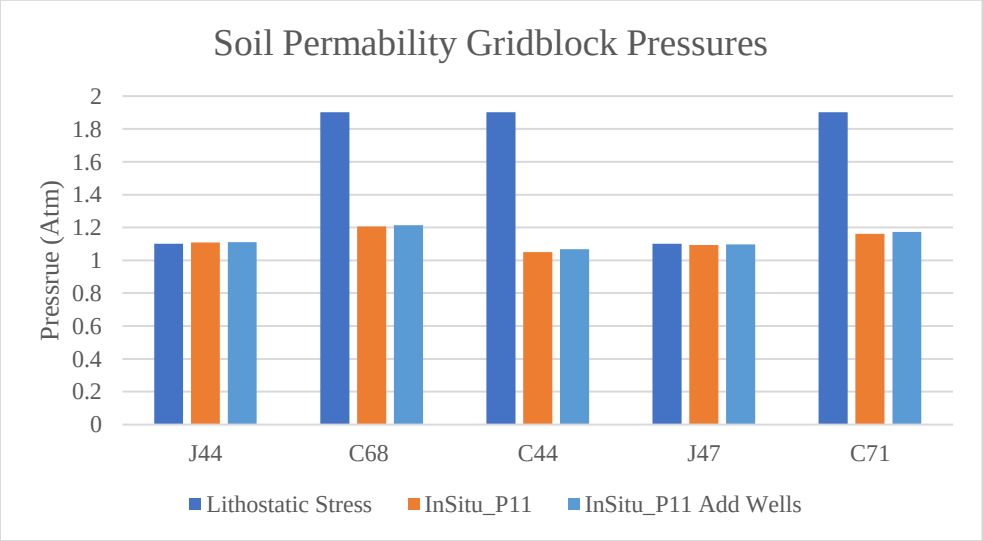

Figure 51: Gridblock pressures comparison in the higher permeability simulation with the addition of wells.

The gridblocks used to record the pressures in the in-situ models were chosen along injection and vacuum wells to record the total pressures under the thermal blanket. The additional wells prevent the lateral migration of mercury and evaporates the mercury fringe that occurred along the hot zone.

5.6 Conclusion

Soil material and soil permeability need to be considered in order to understand airflow and contamination pathways during remediation. Comprehensive soil and geologic characterization will help define the model parameters used to setup laboratory and field-based applications of thermal treatment for elemental mercury.

The injection rate of air and the water saturation were two of the most important parameters discussed in Chapter 5. Injection rates need to be large enough to dewater the volume and prevent new water from wicking up from the watertable. Injection rates must also not exceed the vacuum rate of extraction.

CHAPTER SIX

CONCLUSION AND FUTURE WORK

6.1 Introduction

The overall objectives of this research were to validate the numerical simulator and to design and simulate ex-situ and in-situ thermal treatment for mercury. Validating the numerical simulator was to ensure the TOUGH2/TMVOC's ability to reproduce Kunkel's (2006) mercury laboratory experiments.

Simulations were conducted to simulate the thermal treatment of mercury in highly idealized conditions. One example of a large assumption was the homogeneous, unconsolidated soil used within the models. The simulations were conducted over three different permeabilities to show that air flow must be injected at higher rates in order to penetrate low permeability soil. A large downside to larger injection rates is the pressure that builds up behind the injection. Larger injection rates heat up the volume in a shorter amount of time and as a result remove mercury at a faster rate. When the lithostatic stress of the soil is reached soil fractures can create airflow pathways for vapors. Fracture stress must be considered and injection pressures must not exceed the stress of the soil to ensure that r airflow does not escape the system and release toxic vapor.

6.2 TMVOC Model Validation

The TOUGH2/TMVOC accurately modeled Kunkel's Hg3 experiment for the thermal treatment of mercury (Kunkel et al., 2006). The vapor pressure of mercury needs to be completely understood so that the temperatures within the volume can evaporate mercury.

6.3 Ex-situ Thermal Treatment

The ex situ thermal treatment models for mercury were idealized to assume that the soil was uniformly contaminated with mercury. In a real application of ex-situ treatment, mercury would not be uniformly distributed with the soil. However, ex-situ treatments do involve disturbing large amounts of contaminated soil. Currently, large amounts of excavated soil are placed in landfills. If the soil has to be relocated it is a candidate for ex-situ treatment before transportation. The ex-situ technology incorporates horizontal injection well and SVE wells. The orientation is just one geometry that could be used to inject hot air for the removal of contamination. The large concern in the ex-situ thermal treatment is the material used to enclose the volume of contaminated soil. The ex-situ model contains no flow boundaries that are thermally insulative. In an idealized simulation these conditions are easy to create, however finding a material, or liner, to prevent the escape of mercury under high heat and pressure conditions must be considered.

6.4 In-situ Thermal Treatment

The in-situ thermal treatment for mercury depends on the soil properties of the contaminated soil. The relative permeability and capillary pressure were altered in the model to record the conditions that make the thermal treatment of mercury most effective. Soil that contains mobile phase conditions and low water retention is the most ideal for simulating thermal treatment for mercury.

The three-phase capillary model was adjusted to reduce the amount of residual water within the control volume after gravitational equilibrium. Capillary forces within the model presented problems when additional water wicked into the treatment volume from the watertable. Injection wells need to surround the contaminated areas and provide enough heat energy to evaporate the mercury. The relative permeabilities model was adjusted to study the effects that allow vapor to be the most mobile. As a result, the soil properties need to be highly characterized in order for in situ thermal treatment of mercury to be effective.

Altering the relative permeability and capillary pressure models identified the conditions that remove mercury contamination at reduced pressures. Since soil properties cannot be changed when determining if thermal treatment is feasible the soil properties must then be characterized before the treatment is used. If the soil permeability is relatively high, and the water saturations are low then thermal treatment could be an option to remediate mercury.

6.5 Mercury Feasibility and Future work

The overall effectiveness of using thermal treatment for mercury depends on the environmental assessment of the contaminated site and the potential for contaminant redistribution. The research presented in this work can be refined using an up to date evaluation of the mercury contamination problem at the Oak Ridge National Laboratory. Furthermore, field scale simulations can be conducted considering the modeling sensitivities outline in this work.

REFERENCES

Alloway, B. (2012). Trace metals and metalloids in soils and their bioavailability: Heavy metals in soils.

AMAP/UNEP. (2013). Technical background report for the global mercury assessment 2013. Arctic Monitoring and Assessment Programme.

Bizily, S. P., Rugh, C. L., Summers, A. O., & Meagher, R. B. (1999). Phytoremediation of methylmercury pollution: merB expression in arabidopsis thaliana confers resistance to organomercurials. Proceedings of the National Academy of Sciences of the United States of America, 96(12), 6808-6813.

Brooks, S. C., & Southworth, G. R. (2011). History of mercury use and environmental contamination at the oak ridge Y-12 plant. Environmental Pollution, 159(1), 219-228.

Bucala, V., Saito, H., Howard, J. B., & Peters, W. A. (1994). Thermal treatment of fuel oil-contaminated soils under rapid heating conditions. Environmental Science & Technology, 28(11), 1801-1807.

Chang, T. C., & Yen, J. H. (2006). On-site mercury-contaminated soils remediation by using thermal desorption technology. Journal of Hazardous Materials, 128(2–3), 208-217.

Coats, K. (1977). Geothermal reservoir modelling. Paper presented at the SPE Annual Fall Technical Conference and Exhibition.

Conner, J. R. (1990). Chemical Fixation and Solidification of Hazardous Wastes. Van Nostrand Reinhold, New York, 692, f5.

Crichton, J. (1803). XXV. on the freezing point of tin, and the boiling point of mercury; with a description of a self-registering thermometer invented. The Philosophical Magazine, 15(58), 147-148.

Dalton, J. (1802). On the force of steam or vapor from water and various other liquids, both in a vacuum and in air. Mem.Lit. Philos.Soc. Manchester, 5, 550-595.

de Percin, P. R. (1995). Application of thermal desorption technologies to hazardous waste sites.

Ebadian, M. (2001). Mercury Contaminated Material Decontamination Methods: Investigation and Assessment.

Floess, C. H., Thorpe, M., Hoose, L., & McDonough, S. (2011). Freeman's bridge road site remediation using thermal desorption. Geo-frontiers 2011: Advances in geotechnical engineering (pp. 846-855).

He, F., Gao, J., Pierce, E., Strong, P., Wang, H., & Liang, L. (2015). In situ remediation technologies for mercury-contaminated soil. Environmental Science and Pollution Research, 22(11), 8124-8147.

Hempel, M., & Thoeming, J. (1999). Remediation techniques for hg-contaminated sites. Mercury contaminated sites (pp. 113-130) Springer.

Hicks, W. T. (1963). Evaluation of Vapor-Pressure data for mercury, lithium, sodium, and potassium. The Journal of Chemical Physics, 38(8), 1873-1880.

Hinton, J., & Veiga, M. (2001). Mercury contaminated sites: A review of remedial solutions. Paper presented at the Proceedings of the NIMD (National Institute for Minamata Disease) Forum Minamata, Japan,

Holmes, P., James, K. A. F., & Levy, L. S. (2009). Is low-level environmental mercury exposure of concern to human health? Science of the Total Environment, 408(2), 171-182.

Huber, M. L., Laesecke, A., & Friend, D. G. (2006). The vapor pressure of mercury. Nits, Nistir, 6643.

Hutchison, A. R., & Atwood, D. A. (2003). Mercury pollution and remediation: The chemist's response to a global crisis. Journal of Chemical Crystallography, 33(8), 631-645.

Kabata-Pendias. (2010). Trace elements in soils and plants CRC press Boca Raton.

Kunkel, A. M., Seibert, J. J., Elliott, L. J., Kelley, R., Katz, L. E., & Pope, G. A. (2006). Remediation of elemental mercury using in situ thermal desorption (ISTD). Environmental Science & Technology, 40(7), 2384-2389.

Lewis, G. N., & Macdonald, R. T. (1936). The separation of lithium isotopes. Journal of the American Chemical Society, 58(12), 2519-2524.

Lighty, J. S., Pershing, D. W., Cundy, V. A., & Linz, D. G. (1988). Characterization of thermal desorption phenomena for the cleanup of contaminated soil. Nuclear and Chemical Waste Management, 8(3), 225-237.

Looney, B., Eddy-Dilek, C., Turner, R., Southworth, G., Peterson, M., & Palumbo, A. (2008). Recommendations to address technical uncertainties in mitigation and remediation of mercury contamination at the Y-12 plant, oak ridge, Tennessee. Wsrc-Sti-2008-00212.

Mason, R. P., Choi, A. L., Fitzgerald, W. F., Hammerschmidt, C. R., Lamborg, C. H., Soerensen, A. L., & Sunderland, E. M. (2012). Mercury biogeochemical cycling in the ocean and policy implications. Environmental Research, 119, 101-117.

Massacci, P., Piga, L., & Ferrini, M. (2000). Applications of physical and thermal treatment for the removal of mercury from contaminated materials. Minerals Engineering, 13(8-9), 963-967.

Morris, M. I. (2002). Demonstration of New Technologies Required for the Treatment of Mixed Waste Contaminated with {Ge} 260 Ppm Mercury,

Mulligan, C. N., Yong, R. N., & Gibbs, B. F. (2001). An evaluation of technologies for the heavy metal remediation of dredged sediments. Journal of Hazardous Materials, 85(1), 145-163.

Ochoa-Loza, F. J., Artiola, J. F., & Maier, R. M. (2001). Stability constants for the complexation of various metals with a rhamnolipid biosurfactant. Journal of Environmental Quality, 30(2), 479-485.

Parker, J., Lenhard, R., & Kuppusamy, T. (1987). A parametric model for constitutive properties governing multiphase flow in porous media. Water Resources Research, 23(4), 618-624.

Peterson, M. J., Brooks, S. C., Mathews, T. J., Mayes, M., Johs, A., Watson, D. B., . . . Pierce, E. (2015). Mercury remediation technology development for lower east fork poplar creek. ORNL/SPR-2014/645, Oak Ridge National Laboratory, Oak Ridge, TN.

PMET. (2006). Pittsburg mineral and environmental technology, mercury recovery service, Inc. (MRS). Retrieved from http://www.pmet-inc.com/mercury/.

Pruess, K. (2008). On production behavior of enhanced geothermal systems with CO 2 as working fluid. Energy Conversion and Management, 49(6), 1446-1454.

Pruess, K., & Battistelli, A. (2002). TMVOC, a numerical simulator for three-phase non-isothermal flows of multicomponent hydrocarbon mixtures in saturated-unsaturated heterogeneous media. Report LBNL-49375 Lawrence Berkeley National Laboratory.

Qu, L., FU, S., LIU, L., AN, Y., & LI, M. (2004). A study on the soil improvement polluted by mercury [J]. Journal of Guizhou Normal University (Natural Science), 2, 013.

Reid, R. C. (1987). The properties of gases and liquids (4th ed. ed.). New York: McGraw-Hill.

Saito, H., Howard, J., Peters, W., & Bucalá, V. (1998). Soil thermal decontamination: Fundamentals. The Encyclopedia of Environmental Analysis and Remediation, 7, 4554-4589.

Siebert, J. (2005). An examination of using in-situ thermal desorption to remediate mercury contaminated soils through laboratory experiments and numerical modeling. Unpublished Master's Thesis, University of Texas at Austin.

Sierra, M. J., Millán, R., López, F. A., Alguacil, F. J., & Cañadas, I. (2016). Sustainable remediation of mercury contaminated soils by thermal desorption. Environmental Science and Pollution Research, 23(5), 4898-4907.

Smith, D. R. (2009). Recalling the Y-12 COLEX (column exchange) process. The Oak Ridger, Oak Ridge, TN.

Stegemeier, G. L., & Vinegar, H. J. (2001). Thermal conduction heating for in-situ thermal desorption of soils. Chapter, 4, 1-37.

Stegemeier, G. L., Vinegar, H. J., & De Rouffignac, E. P. (2005). Thermally Enhanced Soil Decontamination Method.

Stepan, D., Fraley, R., & Charlton, D. (1995). Remediation of mercury-contaminated soils: Development and testing of technologies. Gas Research Institute Topical Report GRI-94/0402.

Swenson, D., & Hardeman, B. (2003). Thunderhead Engineering Consultants, Inc., PetraSim, 1006 Poyntz Ave., Manhattan, KS, 66502.

Thomas, G. W. (1982). Principles of hydrocarbon reservoir simulation.

US Department of Energy. (2009). Technology readiness assessment guide. (Guide), 413.3-4.

Wang, J., Feng, X., Anderson, C. W., Wang, H., Zheng, L., & Hu, T. (2012a). Implications of mercury speciation in thiosulfate treated plants. Environmental Science & Technology, 46(10), 5361-5368.

Wang, J., Feng, X., Anderson, C. W. N., Xing, Y., & Shang, L. (2012b). Remediation of mercury contaminated sites – A review. Journal of Hazardous Materials, 221–222, 1-18.

Why, D. (2009). External technical review of the major risk factors integrated facility disposition project (IFDP) oak ridge, TN.

Wilkerson, L. O., DePaoli, S. M., & Turner, R. (2013). Progress and future plans for mercury remediation at the Y-12 national security complex, oak ridge, tennessee-13059. Paper presented at the WM Symposia, 1628 E. Southern Avenue, Suite 9-332, Tempe, AZ 85282 (United States).

Xu, J., Bravo, A. G., Lagerkvist, A., Bertilsson, S., Sjöblom, R., & Kumpiene, J. (2015). Sources and remediation techniques for mercury contaminated soil. Environment International, 74, 42-53.